Lucas García Cillanueva

3D video transmission over LTE

Dissertação de Mestrado

14 de Fevereiro de 2014

FCTUC FACULDADE DE CIÊNCIAS E TECNOLOGIA
UNIVERSIDADE DE COIMBRA

FACULDADE DE CIÊNCIAS E TECNOLOGIA DA
UNIVERSIDADE DE COIMBRA

MESTRADO INTEGRADO EM ENGENHARIA
ELECTROTÉCNICA E DE COMPUTADORES

3D Video Transmission over LTE

Lucas García Cillanueva

Júri

Presidente:	Professor Vítor Manuel Mendes da Silva
Vogal:	Professor António Paulo Mendes Breda Dias Coimbra
Orientador:	Professor Luís Alberto da Silva Cruz

Coimbra, 14 de Fevereiro de 2014

Abstract

This thesis presents a research work on quality of experience in 3D video transmission over LTE networks. The objective is to study the state-of-art of LTE and 3D video, described in the scientific literature, and to quantify the user quality of experience (QoE) during a simulated LTE transmission.

The work will start by a study of the University of Wien "LTE-A System Simulator" and its capabilities. In addition, different scenarios with various users equipment (UEs) and base stations (eNodeBs) densities will be configured and simulated in order to obtain the frame-by-frame Block Error Rate (BLER) values experienced by different UEs.

Once obtained, the Block Error Rate frames will be converted to packet level error traces, which will be used to introduce erasures and corruptions into the packetized 3D video bitstream.

The corrupted encoded video stream will be decoded using an error-concealment capable video decoder and the decoded/recovered video quality (QoE) will be estimated based on the Structural Similarity Index of the recovered video.

Finally, the QoE results for the different system configurations will allow classifying the severity of the QoE degradations due to transmission losses, through inferring the relationship between those system parameters and the achievable QoE.

Keywords: 3D Video, Quality of Experience, Long Term Evolution, Evolved Node B, User Equipment, Block Error Rate, Structural Similarity Index.

Resumo

Esta dissertação apresenta um trabalho de investigação sobre a qualidade de experiência numa transmissão de vídeo 3D sobre redes LTE. O objectivo é estudar o estado-da-arte no que respeita a rede LTE e vídeo 3D, descrito na literatura científica, e obter a qualidade de experiência de usuário (QoE) durante uma simulação de transmissão LTE.

O trabalho começará por um estudo do University of Wien "LTE-A System Simulator" e as suas capacidades. Para este efeito, vão ser configurados diferentes cenários com distintas densidades de utilizadores (UEs) e estações base (eNodeBs), com o fim de obter a taxa de erros do bloco (BLER) experimentada por diferentes utilizadores.

Depois de obter esta taxa, as tramas da taxa de erros do bloco (BLER) serão convertidas em tramas de nível de erro de pacotes, que vão ser usadas para adicionar corrupções de bit em ficheiros de vídeo 3D.

O fluxo de vídeo codificado e corrompido será descodificado usando um descodificador de vídeo e a qualidade do vídeo recuperado vai ser calculada com base no Índice de Similitude Estrutural.

Finalmente, os resultados de QoE para as diferentes configurações do sistema permitirão classificar o nível das degradações de QoE devido a perdas de transmissão, por meio de inferir a relação entre os parâmetros do sistema e a QoE obtida.

Palavras-chave: Vídeo 3D, Qualidade de experiência do Usuário, Evolução de Longo Prazo, utilizador LTE, Taxa de Erros de Bloco, Índice de Similitude Estrutural.

Contents

List of Figures

List of Tables

List of Acronyms and Abbreviations

2D	Two-dimensional
3D	Three-dimensional
3DTV	Three-dimensional Television
3GPP	3rd Generation Partnership Project
ARQ	Automatic Repeat Request
AVC	Advance Video Coding
BS	Base Station
BCH	Broadcast Channel
BLER	Block Error Rate
CQI	Channel Quality Identifier
CRC	Cyclic Redundancy Check
DCCH	Dedicated Control Channel
DIBR	Depth-Image-Based Rendering
DL-SCH	Downlink Shared Channel
DTCH	Dedicated Traffic Channel
EnodeB/eNB	Evolved Node B
EPC	Evolved Packet Core
EPS	Evolved Packet System
FVV	Free Viewpoint Video
H.264/AVC	ISO/ITU Video Coding Standard
HARQ	Hybrid Automatic Repeat Request
HSPA	High-Speed Packet Access
IP	Internet Protocol

LTE	Long Term Evolution
MAC	Medium Access Control
MBMS	Multimedia Broadcast and Multicast Services
MCCH	Multicast Control Channel
MCH	Multicast Channel
MCS	Modulation and Coding Scheme
MIMO	Multiple-Input Multiple-Output
MME	Mobility Management Entity
MPEG	Moving Picture Experts Group
MS	Mobile Station
MTCH	Multicast Traffic Channel
MVD	Multi-view Video plus Depth
OFDM	Orthogonal Frequency Division Multiplexing
PAPR	Peak-to-Average Power Ratio
PCCH	Paging control Channel
PCH	Paging Channel
PDCP	Packet Data Convergence Protocol
PDN	Packet Data Network
PDU	Protocol Data Unit
PHY	LTE Physical Layer
PLCC	Pearson Linear Correlation Coefficient
PLR	Packet Loss Ratio
PSNR	Peak Signal-to-Noise Ratio
QoE	Quality of Experience

RAN	Radio Access Network
RB	Resource Block
RLC	Radio Link Control
ROHC	Robust Header Compression
RX	Receiver
SAE	System Architecture Evolution
SC-FDMA	Single-Carrier Frequency Division Multiple Access
SDU	Service Data Unit
SGW	Serving Gateway
SM	Spatial Multiplexing
SSIM	Structural Similarity Index Model
SU-MIMO	Single User- MIMO
SVC	Scalable Video Coding
TTI	Transmission Time Interval
UDP	User Data Protocol
UE	User Equipment
UL	Uplink
UL-SCH	Uplink Shared Channel
UMTS	Universal Mobile Telecommunications System
UTRAN	Universal Terrestrial Radio Access Network
V+D	Video plus Depth
VQA	Video Quality Assessment
WCDMA	Wideband Code Division Multiple Access

1. Introduction

1.1. Context

Latest developed technologies based in 3D video and image transmission are translated into an increasing consumer demand for 3D content [6]. Recent studies have anticipated that the adaptive streaming portion of Internet video will grow at an average of 77% per year, reaching up to 51% of the network video traffic consumed by 2015. With the main purpose of delivering the best user experience, adaptive streaming has to optimize the video configurations during transmission.

3D video provides more realism of the scene, and it involves much more information needed to transmit the video than the two-dimensional (2D) representation. Thus, current and future networks should be able to dedicate a large amount of bandwidth to 3D video streaming services.

Immersive and interactive multimedia applications over wireless will be enabled by the recent LTE standard, thanks to the low latencies and high data rates supported. LTE emerges as a 3GPP (Third Generation Partnership Project) standard, and enables high transmission data rates by supporting radio access with up to 100Mbit/s in full mobility wide area deployments and 1Gbps in low mobility local area deployments [24]. In terms of the high spectral efficiency, it is located between 5 and 10 b/s/Hz for a single user and for 2 to 3 b/s/Hz for the multiuser case. This enables reliable wireless transmission of huge content over the LTE networks.

The latest broadband cellular technology, LTE, allows supporting different services with high data rates and different Quality of Service requirements. Therefore, it can be considered a very promising architecture for 3D video transmission.

1.2. Outline of the dissertation

Firstly, an overview of LTE technology is presented, with emphasis on the main goals and key features of LTE. Moreover, the network and protocol architectures will be introduced.

Section 3 talks about the LTE Physical Layer, the main LTE layer studied in this work.

In section 4, the state-of-art of the 3D technology is explained. For this purpose, the structure of an end-to-end 3D video system and the different types of the 3D video representations are mentioned. Additionally, the main quality metrics of 3D video are enumerated.

Section 5 provides information about the tools used in this scope, with emphasis on the "University of Wien LTE-A System Simulator", the main tool employed in this investigation.

In section 6, the experimental results are described. This section is divided into two parts: the simulator output results (Packet Loss Ratio results) and the QoE results (Structural Similarity Index results).

This thesis concludes with section 7, by summarizing the results obtained and drawing some conclusions.

2. LTE System Overview

Long Term Evolution (LTE) has been designed to support only packet-switched services, contrary to the prior cellular systems, based on circuit-switched models. The main LTE purpose is to provide IP connectivity between UE (User Equipment) and the PDN (Packet Data Network) without occurring interruptions of user applications during connection.

In LTE there is a big change compared to previous mobile technologies, UMTS (Universal Mobile Telecommunications System) and HSPA (High Speed Packet Access) due to the introduction of a novel physical layer and the core network reform. The main reasons for these Radio Access Network (RAN) system design developments are the requirement to provide higher spectral efficiency, lower delay and more multi-user flexibility and secure service than the existing deployed networks.

Thus, while LTE includes the evolution of the Universal Mobile Telecommunications System (UMTS) Radio Access Network by designing the Evolved UTRAN (E-UTRAN), there is also a development of other aspects, like the System Architecture Evolution (SAE), which covers the Evolved Packet Core (EPC) network. The Evolved Packet System (EPS) is included by the LTE and SAE.

2.1 Key features of LTE

LTE aims to achieve a *peak* data rate of 100 Mbit/s to 326,4 Mbit/s (with ideal conditions) in the downlink and for 50 Mbit/s to 86,4 Mbit/s in the uplink (UL), with a 20 MHz spectrum allocation for *each* of the downlink and uplink. Thus, it is required a spectral efficiency of 5 for the downlink and 2.5 bit/s/Hz for the uplink [3]. Due to the wide range of applications and requirements, LTE defines different types of User Equipment (UE), depending on the antenna configuration and the modulation chosen [4]:

UE category	Peak downlink data rate (Mbit/s)	Downlink antenna configuration (eNodeB transmit x UE receive)	Peak uplink data rate (Mbit/s)	Support for 64QAM in uplink
Category 1	10.296	1x2	5.16	No
Category 2	51.024	2x2	25.456	No
Category 3	102.048	2x2	51.024	No
Category 4	150.752	2x2	51.024	No
Category 5	302.752	4x2	75.376	Yes

Table 1 - Types of Mobiles Stations [4]

For latency, the goals distinguish between:

- *Control-plane latency* (defined as the time for a handset to transition from various non-active states to active states), which are between 50 and 100 ms, depending on the state in which the UE originally was. Furthermore, at least 400 active UEs per cell should be supported.
- *User-plane latency* (defined as the time required to transmit a small Internet Protocol (IP) packet to the edge node of the *Radio Access Network*, RAN), which should not exceed 5ms in a network with a single UE (i.e., no congestion problems).

LTE defined performance requirements into the WCDMA systems, for operation under realistic circumstances. Basically, the main requirement is relative to the user

throughput, that it should improve from 2 to 4 times. Since the main usage, especially for data services, is expected to be for mobile terminals, the LTE system is intended to be optimized for low speeds (to about 15 km/h). Relative to higher speeds, is allowed light performance degeneration for speeds up to 120 km/h, while for really high-speed applications (up to 500 km/h), only basic connectivity needs to be kept.

Due to the need of coexistence of the WCDMA and LTE systems for a considerable number of years, usually in the same frequency band, the transition from both systems should be made as seamless as possible. Transitions/handovers from one system to the other will be frequently required, especially during the initial deployment of LTE, when only parts of the service area will be covered by LTE Base Stations (BSs). Relative to the transition times, for real-time applications it should be less than 300 ms, and for non-real time applications should be less than 500 ms.

Figure 1 represents the evolution of relative subscriptions in mobile technologies since 1990:

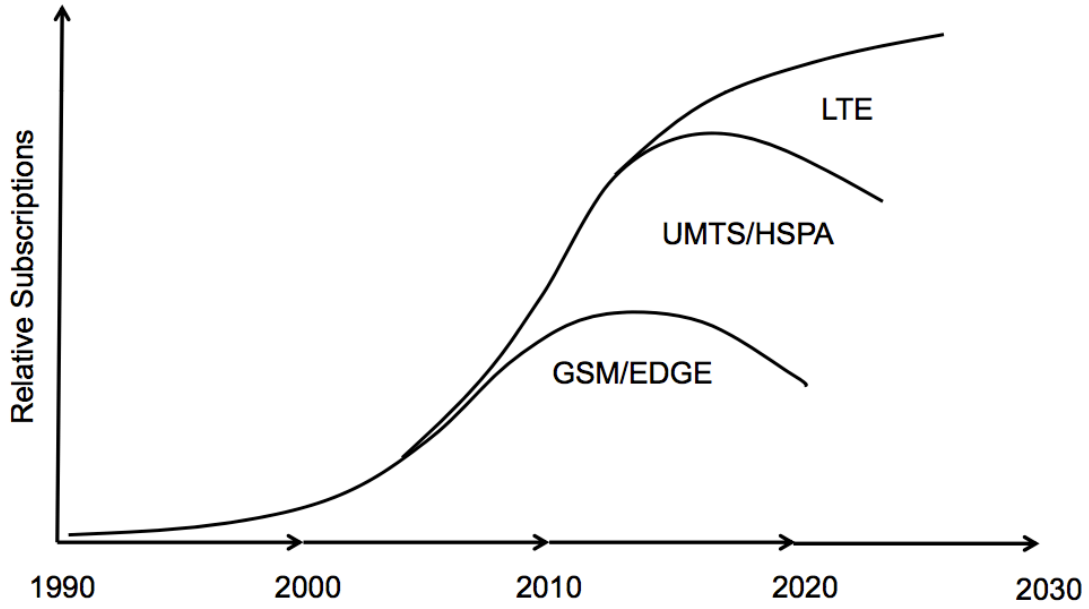

Figure 1 - Relative subscriptions in mobile technologies [26]

2.2. Network architecture

In principle, the LTE network structure is quite simple. Actually, it is simplified with respect to the GSM and WCDMA structure: there is only a single type of access point, the eNodeB (or Base Station, BS). Each BS can support one or more cells, providing the following functionalities:

- Air interface communications and PHYsical layer (PHY) functions
- Radio resource allocation/scheduling
- Retransmission control

The X2 interface is the interface between different BSs. Important information is exchanged through this interface for the coordination of transmissions in adjacent cells (e.g. for reduction of the intercell interference). The S1 interface connects each BS to the core network.

The LTE developed core network, called System Architecture Evolution (SAE) or Enhanced Packet Core (EPC), is based on packet-switched transmission. It consists of a Mobility Management Entity (MME), the serving gateway (connecting the network to the RAN), and the packet data network gateway, which connects the network to the Internet. In addition, the Home Subscriber Server is defined as a separate entity. The core network complies the following functionalities:

- Subscriber management and charging
- Quality of service provisioning, and policy control of user data flows
- Connection to external networks

The network must also provide enough user security and privacy and network protection against fraudulent use. Figure 2 represents the LTE network architecture:

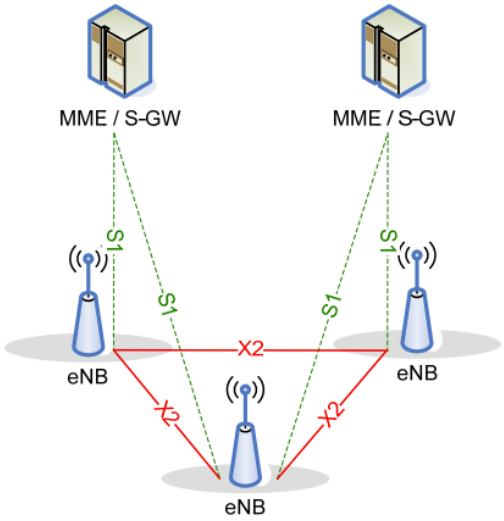

Figure 2 - LTE network architecture [27]

2.3. Protocol architecture

In this section the LTE protocol architecture is explained. Figure 3 shows the different protocol layer that structure the processing specified for LTE:

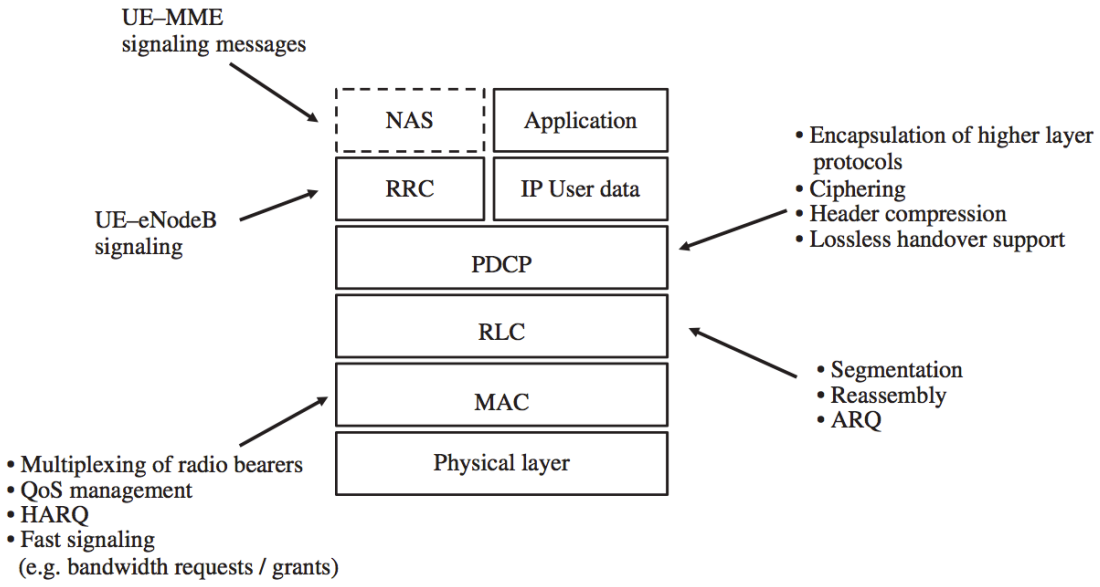

Figure 3 - LTE Protocol stack and main functions [25]

In figure 4 is illustrated a general overview of the LTE protocol architecture for the downlink. Related to the LTE protocol structure of the uplink transmission, it is quite similar to the downlink. However, with respect to multi-antenna transmission and transport format selection there are some differences between them [1].

Prior to transmission over the radio interface, incoming IP packets are passed through multiple protocol entities, enumerated bellow [1]:

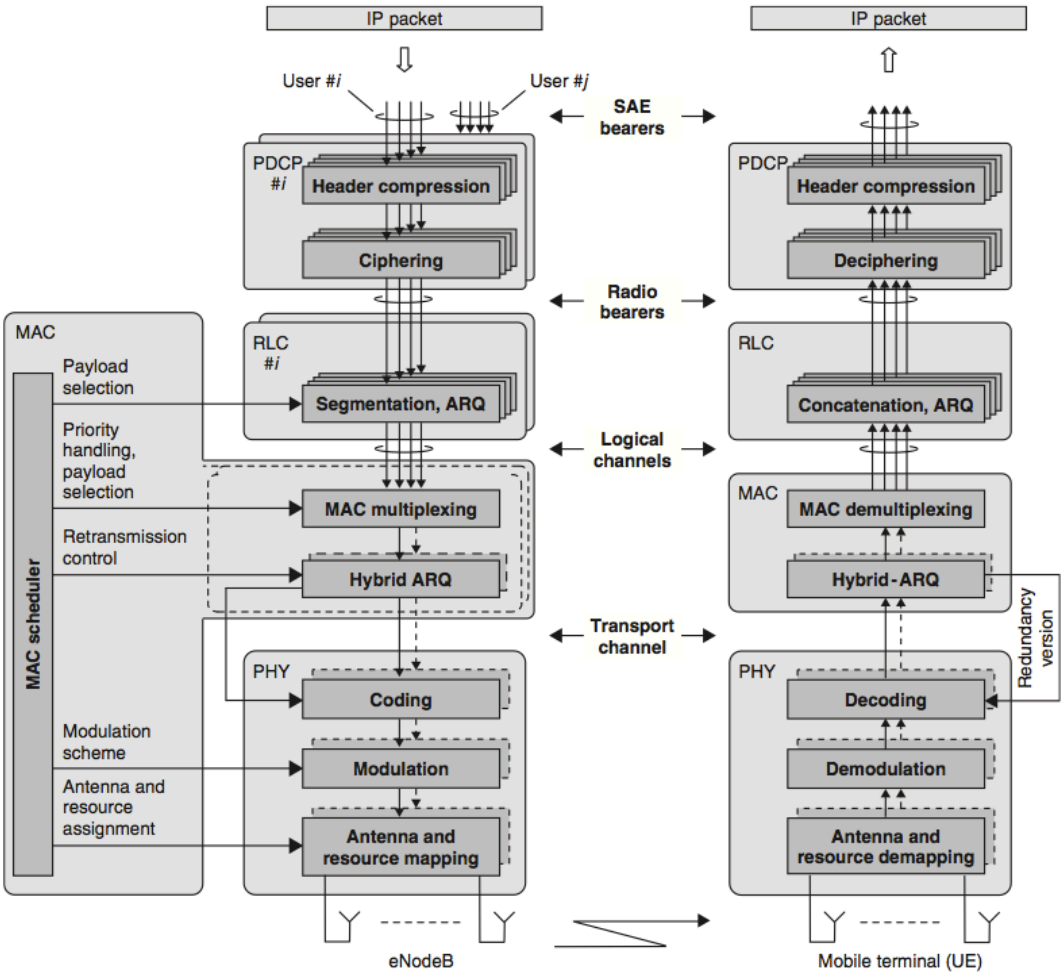

Figure 4 - Overview of the LTE protocol architecture for downlink [1]

- *Packet Data Convergence Protocol* (PDCP) ciphers user and signaling traffic over the radio interface. It ensures the integrity protection of the transmitted data by protecting against attack scenarios. At the receiver side, PDCP performs the

deciphering and decompression operations. PDCP is also responsible of the IP header compression. It is necessary to reduce the number of bits necessary to transmit over the radio interface. The header compression is based on the ROHC algorithm, used in WCDMA as well as other mobile-communication standards.

- *Radio Link Control* (RLC) is responsible for segmentation and reassembly, retransmission handling, and in-sequence delivery for higher layers. The higher layer packets need to be adapted to packet sizes that can be sent over the radio interface. This protocol is located in the eNodeB since there is only a single type of node in the LTE radio-access-network architecture. The RLC offers services to the PDCP in the form of *radio bearers*.
- *Medium Access Control* (MAC) handles hybrid-ARQ retransmissions and uplink and downlink scheduling. The scheduling functionality is located in the eNodeB, which has one MAC entity per cell, for both uplink and downlink. The MAC offers services to the RLC in the form of *logical channels*.
- *Physical Layer* (PHY) handles coding/decoding, modulation/demodulation, multi-antenna mapping, and other physical layer functions. The physical layer offers services to the MAC layer in the form of *transport channels*.

Now the RLC and MAC entities will be explained in more detail.

2.3.1. Radio Link Control

The *Service Data Units* (SDUs) are segmented and concatenated by the RLC into available packets for transmission across the radio channel, named as *Protocol Data Units* (PDUs). The PDU size can be adjusted dynamically, due to the dynamic changes of the transmission data rates.

The RLC also ensures that all PDUs arrive at the receiver (RX) (and arrange for retransmission if they do not), and delivers them to the PDCP in their correct order.

The scheduler decides the amount of data from the RLC SDU buffer should be selected for transmission, and in order to create the RLC PDU, the SDUs are

segmented/concatenated. Hence, during a LTE transmission the PDU size varies *dynamically* [2]. Figure 5 represents the RLC PDU creation.

It is important to note that the large PDU size resulted of high data rates means to a smaller overhead. On the other hand, for low data rates is required a small PDU size.

Hence, as the LTE data rates may oscillate dynamically in a very large range, dynamic PDU sizes are motivated for LTE.

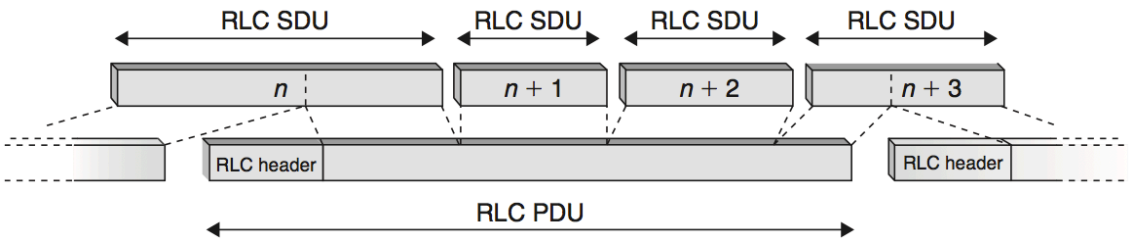

Figure 5 - Radio Link Control PDU

2.3.2. Medium Access Control

The MAC layer provides HARQ (Hybrid Automatic Repeat Request) retransmissions and is responsible for the functionality that is required for medium access, such as scheduling operation and random access.

Logical channels and transport channels

The MAC communicates to the RLC in the form of *logical channels*, as mentioned before. The type of information it carries defines a logical channel. These channels are mainly classified into *control* channels (used for transmission of control and configuration information necessary for operating an LTE system) and *traffic channels* (used for the user data). Hence are enumerated the main logical channels:

- Broadcast Control Channel (BCCH): used for system control information broadcasting from the network to all mobile terminals in a cell.

- Dedicated Control Channel (DCCH): used for transmission of control information to/from a mobile terminal for single configuration.
- Paging Control Channel (PCCH): used for paging of mobile terminals whose location on cell level is not known to the network.
- Multicast Control Channel (MCCH): used for transmission of control information required for multiple reception.
- Dedicated Traffic Channel (DTCH): used for user data transmission to/from a mobile terminal.
- Multicast Traffic Channel (MTCH): used for MBMS services downlink transmission.

The *transport channel* is the format offered to the MAC layer from the physical layer. It is defined by the way the information is transmitted over the network [1]. Data on a transport channel is organized into *transport blocks*. The content of each transport block is the set of bits collected in each Transmission Time Interval (TTI). The types specified for transport channel are:

- Broadcast Channel (BCH): used for broadcasting the information on the BCCH logical channel.
- Paging Channel (PCH): used for transmission of paging information on the PCCH logical channel.
- Multicast Channel (MCH): used to support MBMS. It should be diffused throughout the hole cell.
- Downlink Shared Channel (DL-SCH): used for downlink data transmission. It supports hybrid ARQ, scheduling in the time and frequency domains, and spatial multiplexing (MIMO).
- Uplink Shared Channel (UL-SCH): is the uplink counterpart to the DL-SCH.

Downlink scheduling

In the LTE radio access, time/frequency resources are shared between network users during transmission *dynamically* both in uplink and downlink. The main target of the

scheduler is controlling the assignment of uplink and downlink resources. It is important to know that downlink and uplink scheduling are separated in LTE, because it means that schedule decisions of uplink and downlink transmission can be taken independently of each other.

The downlink scheduler has to determine, in each 1 ms, which terminal(s) that are waiting to receive transmission and the needed resources to reach this. It is possible to have one DL-SCH per scheduled terminal, in which case each terminal is dynamically mapped to a group of frequency resources. Thus, multiple terminals can be scheduled in parallel. The scheduler is also responsible for selecting the modulation scheme, the antenna mapping and modulation scheme. Moreover, the scheduler also controls the data rate, so it decision will affect the RLC segmentation and MAC multiplexing [1].

Information about the downlink channel conditions, critical for channel-dependent scheduling, is sent from the mobile terminal to the eNodeB via Channel Quality Indicator (CQI). It includes information necessary to determine the right antenna processing in case of spatial multiplexing.

Uplink scheduling

The uplink scheduler has to determine, for each 1 ms interval, which mobile terminals (UEs) are to transmit data on their UL-SCH and on which uplink resources (similar to the downlink scheduling basic function).

Thus, the time/frequency resource units are the shared resource controlled by the eNodeB uplink scheduler. In addition, it is important to note that an already assigned resource not fully utilized by a mobile terminal cannot be partially utilized by another mobile terminal [1].

Another important feature in the uplink scheduling decision is that it is taken per mobile terminal (and not per radio bearer). Thus, the terminal should select from which radio bearer the data is taken.

Data flow

Figure 6 shows an example [1] of the flow of downlink data through all the protocol layers, for a case with three IP packets (two on one radio bearer and one on another radio bearer). The required information for deciphering in the terminal is included in the PDCP header.

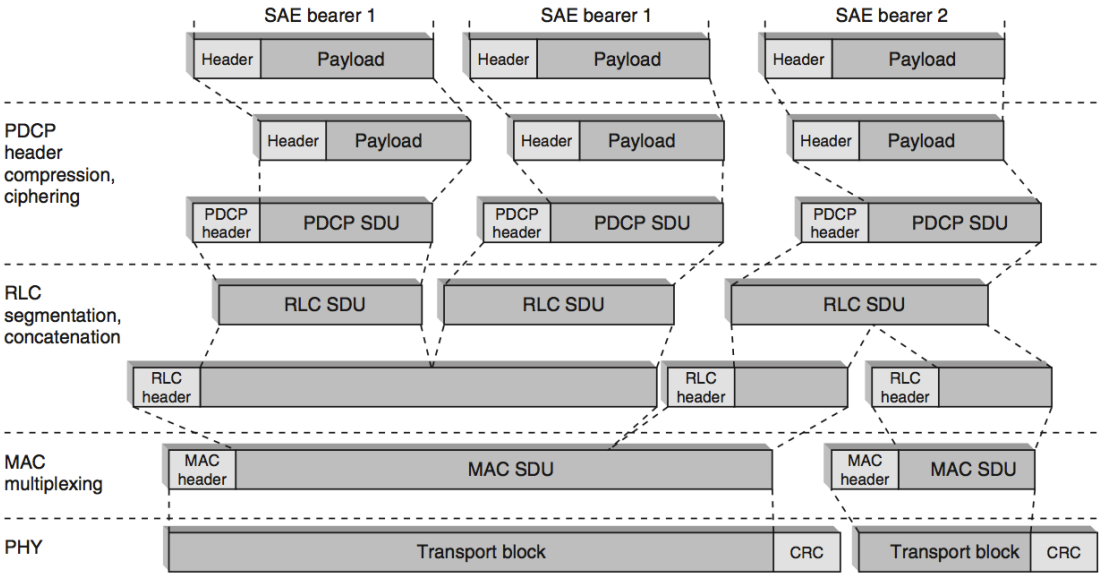

Figure 6 - Flow of downlink data through all the protocol layers [1]

The figure shows that each protocol sub-layer adds its own protocol header to the data units, and how the RLC protocol performs concatenation and/or segmentation of the PDCP SDUs and adds and RLC header. The MAC layer forwards the RLC PDUs, and assembles them into a MAC SDU. Then attaches the MAC header to form a transport block. Depending on the instantaneous data rate selected, the size of this transport block will vary. After that, the physical layer adds a CRC (Cyclic Redundant Check) in order to detect errors. Besides that, this layer performs modulation and coding and transmits the signal over the network. The next chapter provides more information about this layer.

3. LTE Physical Layer

"The physical layer is responsible for coding, physical-layer hybrid-ARQ processing, modulation, multi-antenna processing, and mapping of the signal to the appropriate physical time–frequency resources. It also handles mapping of transport channels to physical channels" [2].

3.1. LTE frame structure

LTE employs OFDM for downlink data transmission and SC-FDMA for uplink transmission. In the next section both modulation techniques will be approached.

3.1.1. OFDMA

OFDMA is considered the main multiplexing scheme in the LTE downlink. This is a technology that allows multiple access by dividing the channel into a group of orthogonal subcarriers, scattered in other sub-groups according to the each user needs.

Relative to the resource scheduling, OFDMA added complexity; however, its improvements result OFDMA to be much better than the current schemes in terms of network latency and efficiency [5].

As mentioned before, the main key in OFDMA is the signal orthogonality. This allows mixing several signals in transmission and then separating it in reception without any interference between them.

In OFDMA, users are allocated a specific number of subcarriers for a predetermined amount of time. These are named as physical Resource Blocks (RBs). The eNodeB scheduler is the responsible for handling the RBs allocations.

In LTE, the time is divided into entities [3]:

- A radio frame, which has duration of 10 ms, is the fundamental time unit of LTE transmission.
- Each radio frame is divided into 10 sub-frames of 1 ms long. These sub-frames are the most LTE processing fundamental time unit.
- Each sub-frame is consisted of two slots (each being 0.5 ms long).
- Each slot is consisted of 6/7 symbols.

We can show this hierarchy in figure 7:

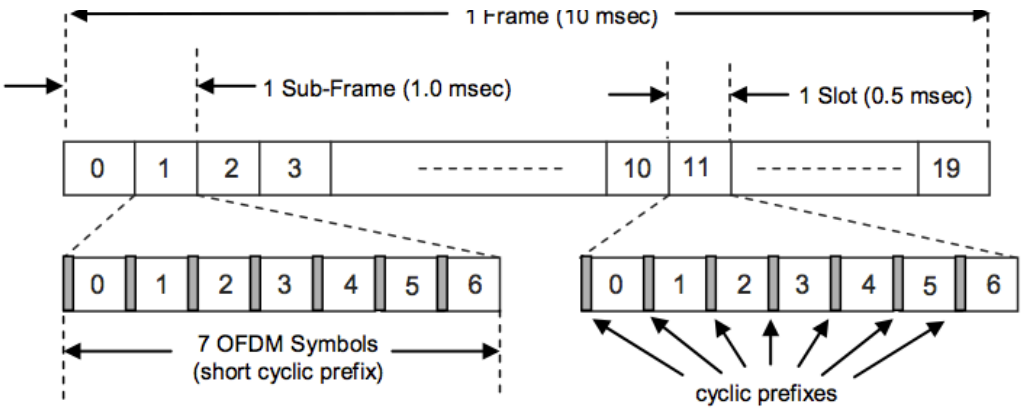

Figure 7 - LTE Generic Frame Structure [5]

Depending on the overall transmission bandwidth of the system, it will be a different number of subcarriers available to transmit/receive. The transmitted downlink signal is consisted of N_{UL} subcarriers for duration of N_{symb} OFDM symbols. A resource grid can represent it, like it is shown in figure 8. The resource element represents a single subcarrier for one symbol period within the grid.

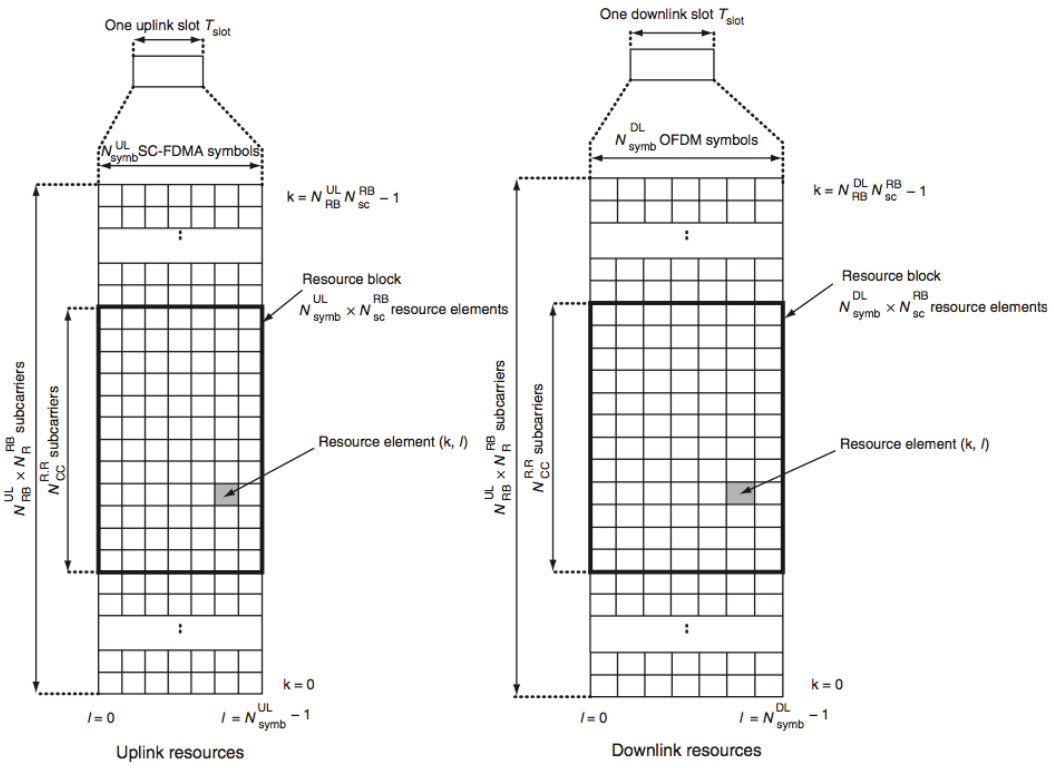

Figure 8 - Resource blocks for uplink and downlink

Figure 9 represents cleaner the relationship between RBs y resource elements:

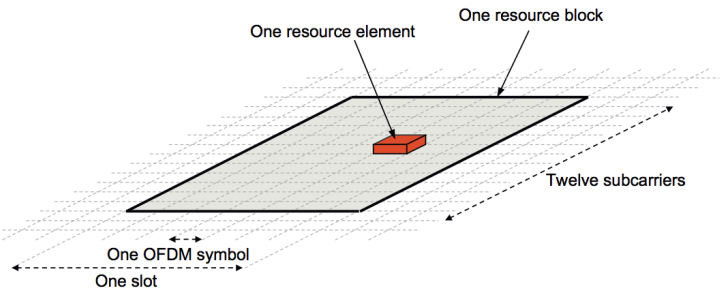

Figure 9 - LTE resource block vs. resource element [2]

As described before, groups of 12 adjacent subcarriers are grouped together on a slot-by-slot basis to form resource blocks (RBs).

3.1.2. SC-FDMA

LTE uplinks requirements are different from downlink, due to the different nature of the UE terminals. For example, power consumption is one of the most important topics during uplink transmission. Due to the loss of efficiency associated with OFDMA signaling, Single Carrier – Frequency Domain Multiple Access (SC-FDMA) is well suited to the LTE uplink requirements.

SC-FDMA presents the same advantages than OFDMA. However, the SC-FDMA signal represented by the subcarrier is single, because the SC-FDMA subcarriers are not independently modulated (unlike OFDMA). As a result, the Peak-to Average Power Ratio (PAPR) is lower than for OFDM transmissions [5].

Due to the project approach is focused on the downlink data transmission, the uplink scheduler won't be mentioned in greater detail.

3.2. Multi-Antenna techniques

In order to reach the aggressive LTE performance targets, the main key performance of this technology is the use of more than one single antenna during transmission.

Multiple antennas can be used in different ways to achieve different aims:

- Multiple antennas at the transmitter and/or the receiver can be used for receive diversity.
- Multiple transmit antennas at the base station can be used for transmit diversity and different types of beam forming.
- Spatial multiplexing, also referred to as MIMO (Multiple Input – Multiple Output), using multiple antennas at both the transmitter and receiver.

The different multi-antenna techniques are beneficial in distinct scenarios, where multiple antennas at the transmitter side should be used to increase the SNR (Signal to Noise Ratio) by means of beam forming [1].

3.2.1. Multiple transmit antennas

By applying multiple antennas at the transmitter side, diversity and beam forming can be achieved. The use of multiple transmit antennas is mainly of interest for the downlink (at the base station). In this case, the use of multiple transmit antennas provides a chance for diversity and beam forming without the need for additional receive antennas and corresponding additional complexity at the terminal [2].

Transmit-Antenna Diversity

If there is no knowledge available of the downlink channels of the transmit antennas at the transmitter, this technique cannot provide beam forming but only diversity. In this case, there should be low mutual correlation between the channels of the different antennas. This technique can be shown in figure 10.

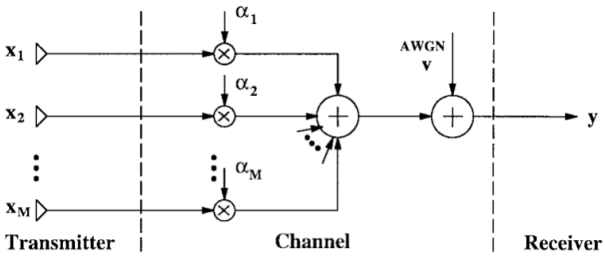

Figure 10 - Diversity channel with an M-element transmit antenna array [29]

Transmitter-Side Beam Forming

Multiple transmit antennas can also provide beam forming in case that there is some knowledge available of the downlink channels of the different transmit at the transmitter side.

A small inter-antenna distance configuration means generally high mutual correlation. Thus, in this case the channels between a receiver and the different transmit antennas are basically the same. In figure 11 it can be shown.

Thus, applying different phase shifts to the signals to be transmitted on the transmit antennas allows handle the transmission beam.

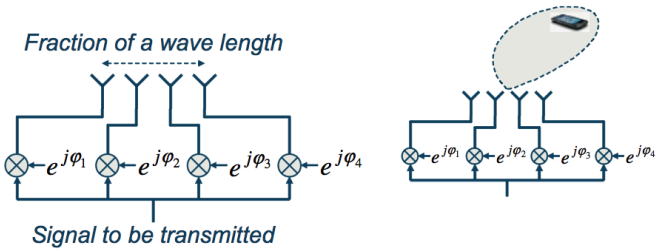

Figure 11 - Classical beam-forming with high mutual antennas correlation [2]

3.2.2. Spatial multiplexing

In the scenario of multiple antennas at the transmitter and the receiver, also emerges the possibility for the spatial multiplexing. It makes a more efficient use of the Signal-to-

Noise and Signal to Interference ratios and allows higher transmission data rates over the LTE radio interface [2].

Under certain conditions [2], attempting to avoid the saturation in the data rates is possible to increase the channel capacity with the number of antennas.

Closed-Loop Spatial Multiplexing

In closed-loop spatial multiplexing, the *codewords* (the parsed output of the decoders) are mapped onto the layers by the next procedure [3]:

- If the number of codewords equals the number of layers, then each layer simply contains the symbols from one codeword.
- If there is one codeword and two layers, then the symbols of the codeword are alternatingly assigned to layer 1 and layer 2.
- If there are 2 codewords and 4 layers, then symbols from codeword 1 are alternatingly assigned to layer 1 and 2, while symbols from codeword 2 are alternatingly assigned to layer 3 and 4.

Open-Loop Spatial Multiplexing

In the case that is not available a feedback of the desired beam forming, this multiplexing can be used [3].

Downlink Multi-User MIMO

MIMO (Multiple Input – Multiple Output) intends to exploit the spatial multiplexing by suppressing the interference between the different layers. MU-MIMO (Multi-User MIMO) is a MIMO extension. SU-MIMO (Single User MIMO) attends to improve the link between base station and user features, while MU-MIMO pretends the coexistence

of several different users sharing the same frequency range. For this purpose, MU-MIMO attempts to exploit a possible spatial decouple between the data flow transmitted and each user for, if it is possible, reach better data rates and efficiency.

Summary, SU-MIMO aims to improve the link capacity while MU-MIMO pretends to increase the cell capacity. Figure 12 represents a downlink transmission from a cell to one or more UEs in MU-MIMO configuration.

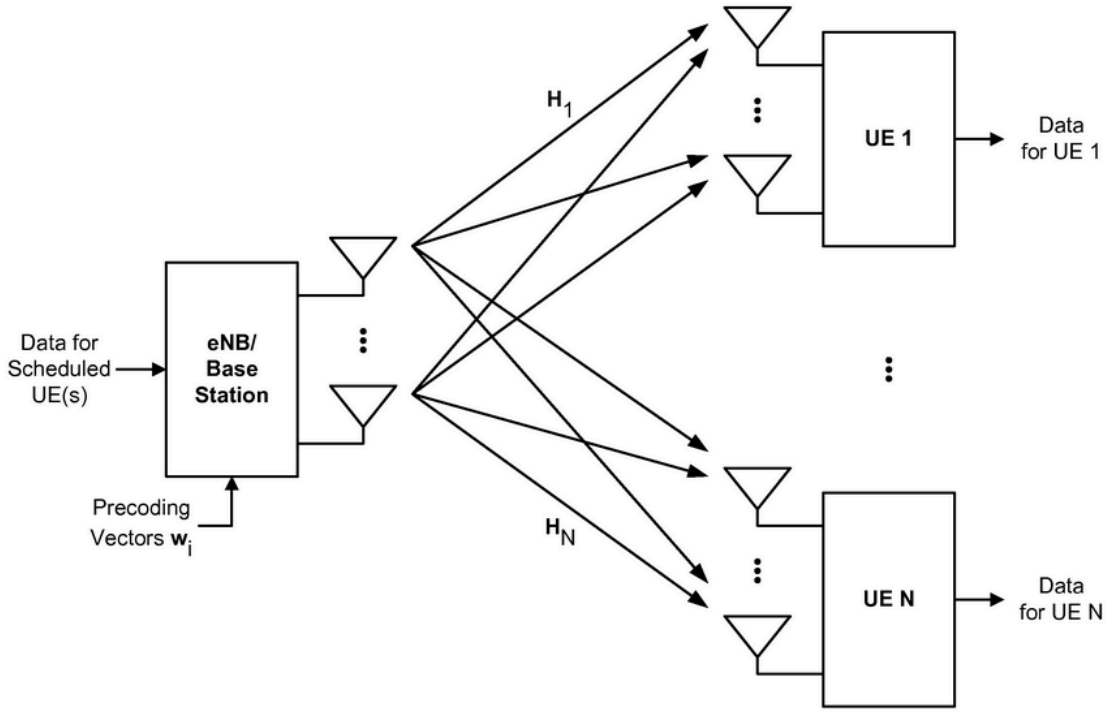

Figure 12 - Downlink transmission in MU-MIMO configuration [28]

4. 3D Video transmissions

4.1. State-of-art

The goal of any multimedia delivery system is to ensure the best video end quality possible, and to achieve this purpose the video created has not to be degraded when it is delivered to the consumer.

Nowadays, 3D video is revolutionizing the audiovisual industry due to the immersion sensation that it produces. Current generation of digital video carries revolutionary aspects as the emergence of new data types in the media.

Many applications are adopting 3D video, and this has resulted in a considerable impact on the market. The need for extending the visual sensation to the 3D (three-dimension) is believed to grow, thus it brings the nearly development and distribution of contents, 3D video processing capable devices and 3D video encoding/decoding standards. Indeed, two main applications refer to 3D video: 3DTV and FVV (Free Viewpoint Video).

3DTV application reaches the 3D perception by fusing two displayed images (one for each eye but from two slightly different viewpoints). It makes the human vision system to assess depth.

In FVV application the user is free to select the desired viewpoint of the displayed scene, thus this furnishes interactivity.

Nowadays, three-dimensional (3D) video representation is one of the technologies that are having greater popularity. A 3D video provides the illusion on the depth perception, thus adding an increased degree of realism to the human eye reception. It gives in fact a value added to the consumer experience.

Due to this reason, 3D video is expected to be the most adopted in the next years in many application fields (e.g. medicine, entertainment, etc.). Actually, recent studies pointed that 3D video is one of the most active research topic nowadays.

4.2. 3D video system

Depending on the targeted application, different representations are available for 3D video and should be rightly chosen.

A 3D content can be provided by a 3D video system in different forms, depending on the input source, the desired quality level, the type of acquisition and scene geometry, the kind of application and the bandwidth [8].

A 3D video system is subdivided into four main groups, as represents figure 13:

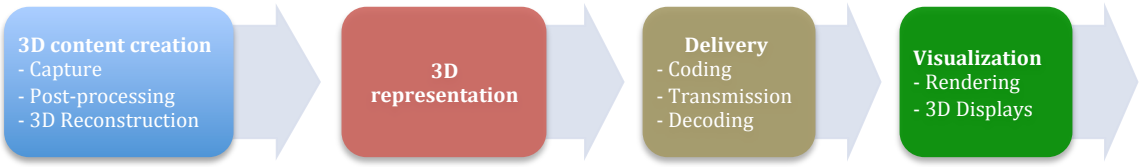

Figure 13 - Structure of an end-to-end 3D video system

4.2.1. 3D content creation

This block is the responsible for providing the data that will be used to set up the 3D video. Firstly the data is captured. Then, it is sent to post-processing, where some algorithms are applied to improve accuracy. Once the data is processed, it is sent to the 3D reconstruction phase, that has the task of creating the data transmitted during the 3D video representation. For more details, see [9].

4.2.2. 3D representation

There are different types of 3D scene representation, depending on the target application and capture devices. They can be classified as in image- and geometry-based formats and also hybrid representation based on the depth maps, which is a combination of image and geometric aspects.

Image-based representation

The most widespread approach makes use of a couple of cameras that capture separately, like human eyes, left and right images. It is a stereoscopic video format composed by two video signals, one for each eye. It is the format used by movie theaters and current 3DTV for home entertainment. The two video signals can be encoded by performing temporal or spatial interleaving. Then, a single frame is formed by the right and left eye images [9]. It can be shown in figure 14. The balls represent the eyes (right and left) and the "blue box" forms the video screen.

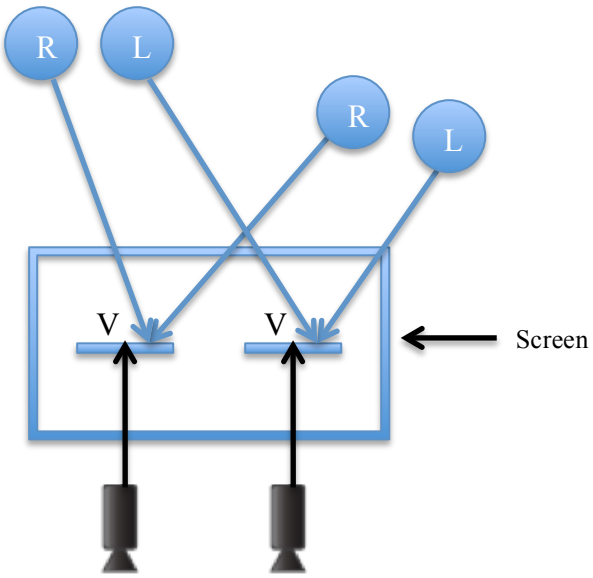

Figure 14 - Image-based representation

Geometry-based representation

Is the extension from 2D to 3D, where the data is represented by voxels instead of pixels. This kind of representation is mainly used in computer-generated graphics for gaming or medical purposes.

Depth maps-based representation

A representation of a point in 3D-space in this case consists in a three-dimensional vector. The depth expresses, in fact, this third coordinate.

The most important development in 3D video is the depth perception, compared to the conventional (2D) video. However, it has a disadvantage: its transmission requires the additional information to be sent as well as more bandwidth and a lower loss probability [10].

A depth map is a gray scale image describing the depth position of the objects using a gray scale typically ranging from white (the closest to the display plane) to black (the farest from the display plane). In it, the distance from the sensor to a visible point at the scene is represented by each pixel.

There are different coding and transmissions arrangements, from the simple video-plus depth simulcast to the complex multiview-plus-depth format (MVD). These two formats will be mentioned in this work.

The video-plus-depth (V+D) format consists in a 2D conventional color video (texture) and an associated depth-map. Each of these depth-images stores depth information, resulting from an 8-bit gray scale quantization. These 256 gray scale values can create a smooth gradient of depth within the image. In order to reconstruct the second view sub-frame, the decoder will use the frames and their depth-map. This is carried out by using Depth Image-based Rendering (DIBR) techniques (see [8] for more details).

Figure 15 shows the DIBR procedure:

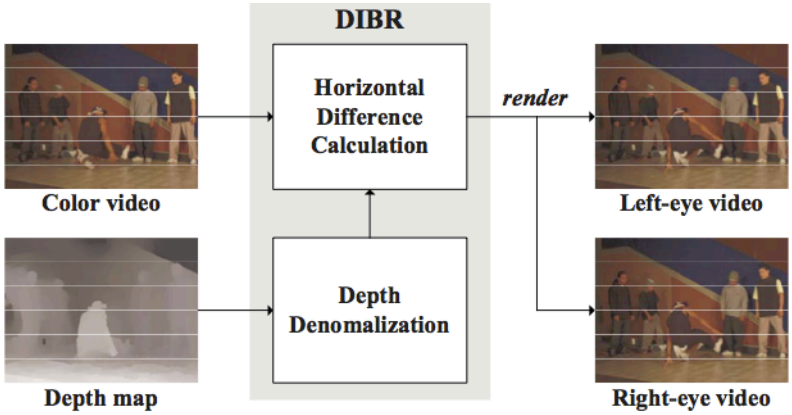

Figure 15 - DIBR procedure [12]

The multiview-plus-depth format (MVD) can be considered as a multiple 2D videos used with their associated depth video, providing more V+D streams. It requires a complex procedure.

Figure 16 represents a MVD system:

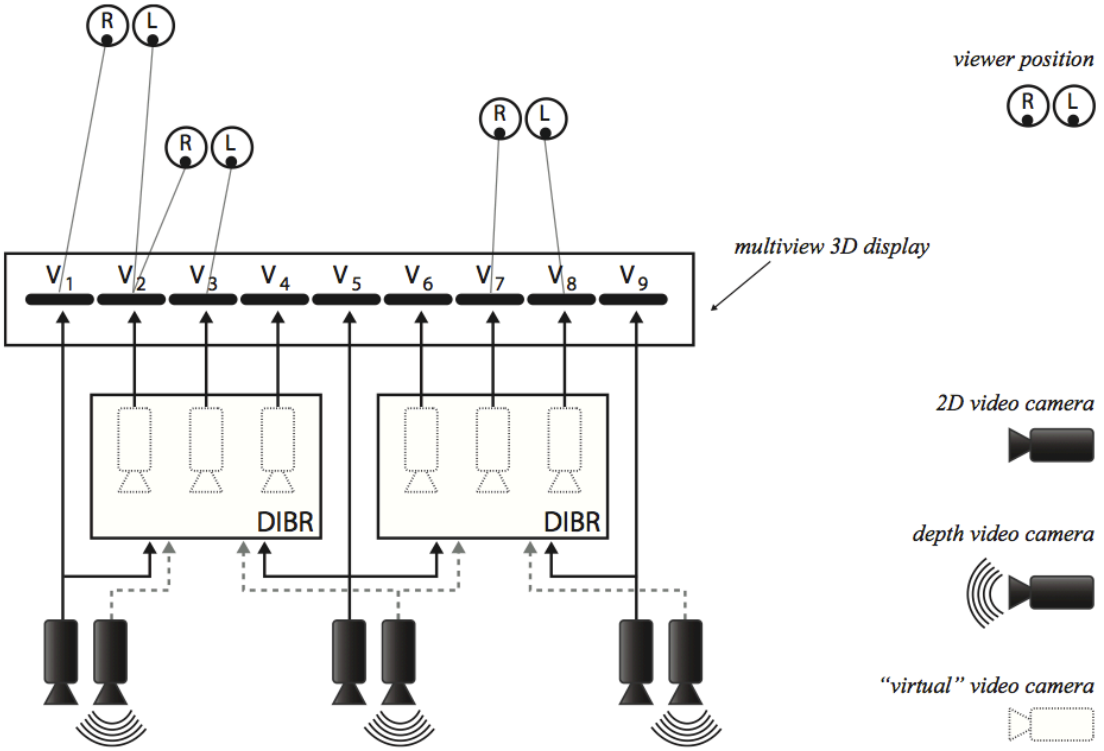

Figure 16 - MVD System [15]

The depth-based representation is widely used in research, standardization and industry [13], because it comprises a number of advantages [11]:

- According to personal preferences of the viewer, it offers the possibility of a customized 3D experience, with either stereoscopic or autostereoscopic displays.
- Efficient compression (high compressed ratio): noise-free depth maps can be represented with only up to 25% of the texture bitrate, making 3D video format based on texture complemented with depth information compatible with the current transmission bandwidth.
- Ability to render virtual views.

4.2.3. Delivery

3D video coding, transmission and decoding are carried out in this stage. Before being transmitted over the network, it is often necessary to compress the 3D video. It is important to know that the highest compression efficiency is one that removes less important information from the video stream.

The H.264/AVC (Advance Video Coding) compression standard with Scalable Video Coding (SVC) extensions is one of most extended compression standard (actually, there is another one better, HEVC), and it is highly used, so in this work only this video codec will be mentioned. It is shown that H.264 increases coding efficiency by approximately 50% compared to previous MPEG standards [14]. LTE networks need to support mobile devices with different displays resolution requirements like small resolution mobile phones and high-resolution laptops. Recognizing this trend, the SVC extension of H.264 allows efficient temporal, spatial and quality scalabilities.

4.2.4. Visualization

This building block is the most important to the end user, because it takes care of the visualization of the 3D video. Its stages are rendering and 3D displays.

The rendering stage employs algorithms to convert the data stored at the representation format. Due to the FVP functionalities and 3D displays needs, the rendering stage focuses on the view synthesis methods.

3D displays are responsible for depth perception of 3D videos. Since 3D media became more accessible to home users, these are in constant development. Recent studies predict that in 2015 more than 30% of all high definition panels at home will have 3D capabilities [9].

4.3. Objective quality metrics of 3D video

In terms of quality control, performance evaluation and resource allocation, is critical to have a good objective video quality assessment (VQA) in a 3D video transmission system.

Visual applications have greatly evolved especially during last years. This has led to a large growth of the demand for video quality assessment technologies [19].

Until now the objective and subjective quality metrics of 2D video has been a constant research topic. However, since the 3D technologies are emerging, it is required new quality assessments and methodologies due to the critical differences in the human visual perception and the typical distortions of the 3D video content.

Due to the availability of several image and 2D video public databases, with common or different features (e.g. spatial resolution, severity of distortions, etc.), to perform realistic comparisons between different objective quality metrics is very difficult.

The work [11] describes the state-of-the art quality metrics for 3D image and video, and the overall conclusion is that it is very difficult (or even impossible) to compare the performance of two different 3D quality evaluation algorithms; every quality metric has its pros, cons, objectives and application scope.

Objective metric quality measures have to provide an indication of quality close to the subjective indication given by the observers. The Pearson Linear Correlation Coefficient (PLCC) is the most used metric in order to evaluate the performance of objective video quality model. For N data pairs (x_i, y_i), with $\bar{x}$ and $\bar{y}$ being the means of the respective data sets, the PLCC is given by:

$$(1) \qquad PLCC = \frac{\Sigma_{i=1}^{N}(x_i-\bar{x})(y_i-\bar{y})}{\sqrt{\Sigma_{i=1}^{N}(x_i-\bar{x})^2} * \sqrt{\Sigma_{i=1}^{N}(x_i-\bar{x})^2}} \in [-1,1]$$

Table 2 shows the PLCC performance comparison of VQA algorithms:

Database	VQEG	IRCCyN	EPFL-PoliMI	LIVE
PSNR	0.7683	0.4160	0.7351	0.5621
SSIM [20]	0.8215	0.5012	0.6781	0.5444
VQM [21]	0.8170	0.4850	0.8434	0.7236
MOVIE [22]	0.8210	0.4850	0.9210	0.8116
Yu *et al.* [23]	0.8170	0.7680	0.9470	0.8450
3D-SSIM [19]	0.8403	0.8194	0.9621	0.8353

Table 2 - PLCC performance comparison of VQA algorithms [19]

In the next section the SSIM (Structural Similarity Index) will be introduced.

4.3.1. Media-layer FR image quality models

There are several models to evaluate the quality of an image reference to the original, but the two most widely known are the Peak Signal to Noise Ratio (PSNR) and the Structural Similarity Index (SSIM) [11].

PSNR can be defined as:

$$(2) \qquad PSNR = 10\, log_{10} \frac{(2^n-1)^2}{MSE}, \text{ with } MSE = \frac{1}{N}\sum_{i=1}^{N}(x_i - y_i)^2$$

where N is the number of pixels of the original image $\boldsymbol{x}$ and the distorted image y, and n is the number of bits per pixel (typically 8). For application-generic purposes, since the MSE does not reflect the way that human visual systems perceive image degradation, this measure has poor correlation with perceived image quality.

On the other hand, to extract structural information from visual scenes, the HVS (human visual systems) is highly adapted. However, its disadvantage is that, given the large volume of video data being transmitted everyday, they are extremely slow and expensive.

A measurement of structural similarity should provide a good approximation to perceptual image quality. For this purpose, the SSIM evaluates image similarity based on three factors computed from the two images being compared [11]: luminance *l(x,y)*, contrast *c(x,y)* and structure *s(x,y)*, defined as:

$$(3) \quad l(x,y) = \frac{2\mu_x\mu_y + C_1}{\mu_x^2 + \mu_y^2 + C_1} \quad , \quad c(x,y) = \frac{2\sigma_x\sigma_y + C_2}{\sigma_x^2 + \sigma_y^2 + C_2} \quad , \quad s(x,y) = \frac{\sigma_{xy} + C_3}{\sigma_x\sigma_y + C_3}$$

where x and y are the reference and the distorted image luminance pixel values, μ and σ represent the mean and the standard deviation, and C_1, C_2 and C_3 are small constants added for numerical stability. By combining these three factors, the overall similarity measure is inferred:

$$(4) \quad SSIM\ (x,y) = [l(x,y)]^{\alpha} \cdot\ [c(x,y)]^{\beta} \cdot\ [s(x,y)]^{\gamma}, \quad \{\alpha,\beta,\gamma\} > 0$$

The score provided by the SSIM ranges between 0 and 1; the closer to 1, the higher the similarity of the distorted image to the reference image and so in this context the better the quality of the image. In this work this quality model will be the used.

5. Methods, tools and simulated scenario

In this work was performed an evaluation of the effect of losses of compressed 3D video transmitted over an LTE system.

For this purpose, the "LTE-A System Level Simulator" of the University of Wien was the main tool used in order to obtain the frame-by-frame Block Error Rate (BLER) values experienced by different UEs.

Thus, using this simulator is possible to obtain the BLER of each transmission time interval (TTI) during the simulation. The selected UE describes a path, and every on millisecond his BLER (Block Error Rate) will be stored into a trace. Figure 17 describes this procedure:

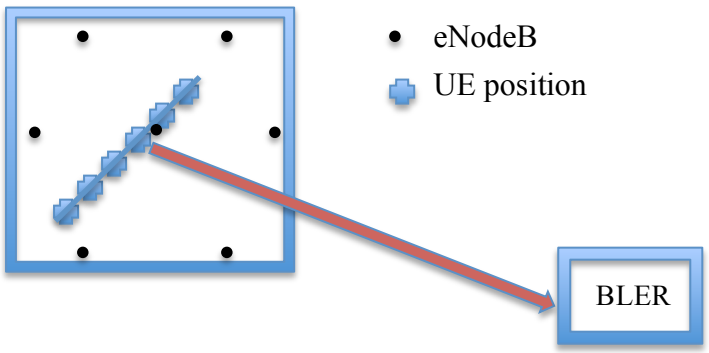

Figure 17 - Simulated scenario

In this chapter an overview of this simulator will be described.

5.1. The University of Vienna System Level LTE Simulator

In order to evaluate the performance of new mobile network technologies, system level simulations are crucial. They aim at determining whether, and at which level predicted link level gains impact network performance [16].

This simulator evaluates the performance of the Downlink Shared Channel of LTE SISO and MIMO networks using Open Loop Spatial Multiplexing and Transmission Diversity transmit modes (mentioned before in this work).

In addition to the System-Level simulator, there is another LTE simulator: the "LTE Link-Level Simulator" [17]. Using both simulators it is possible to obtain results where the results of physical and link-level are isolated from each one and is easier to investigate the performance of the network.

After studying both simulators, the System-Level was chosen because using the Link-Level simulator is not possible to reflect the effects of issues, such as cell planning, scheduling, or interference.

Figure 18 shows the schematic block diagram of the simulator:

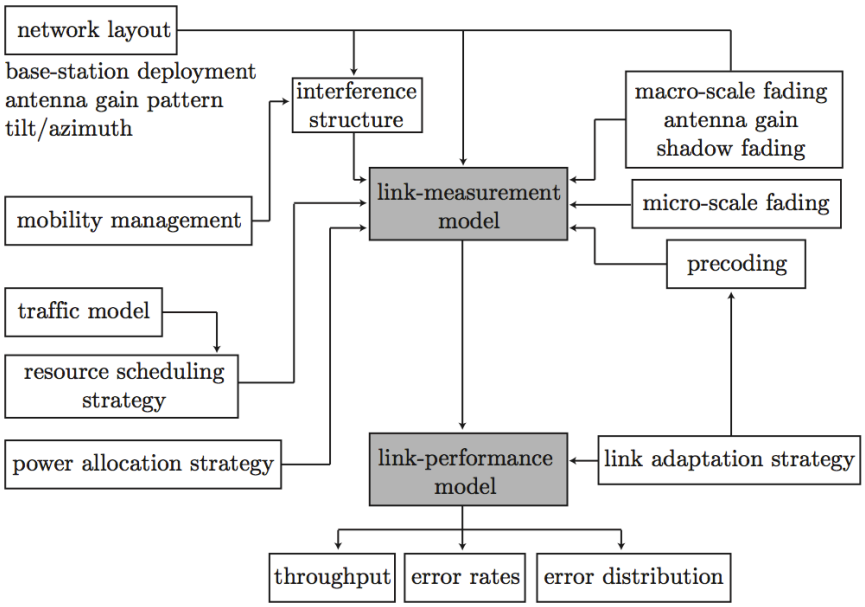

Figure 18 - Schematic block diagram of the simulator [16]

The simulator outputs traces containing throughput and error rates, from which their distributions can be computed.

The link measurement model is focused on the measured link quality used for resource allocation and link adaptation. Moreover, the link performance model is responsible for the determination of the Block Error Ratio (BLER) at the receiver given a certain resource allocation and Modulation and Coding Scheme (MCS).

For LTE are defined different MCS, driven by 15 Channel Quality Indicator (CQI) values. This CQI values use coding rates between 1/13 and 1 combined with 4-QAM, 16-QAM and 64-QAM modulations. (In this work only 16-QAM was used).

Figure 19 represents the CQI vs BLER curves on the left, and the CQI obtained from the 10% BLER points (right).

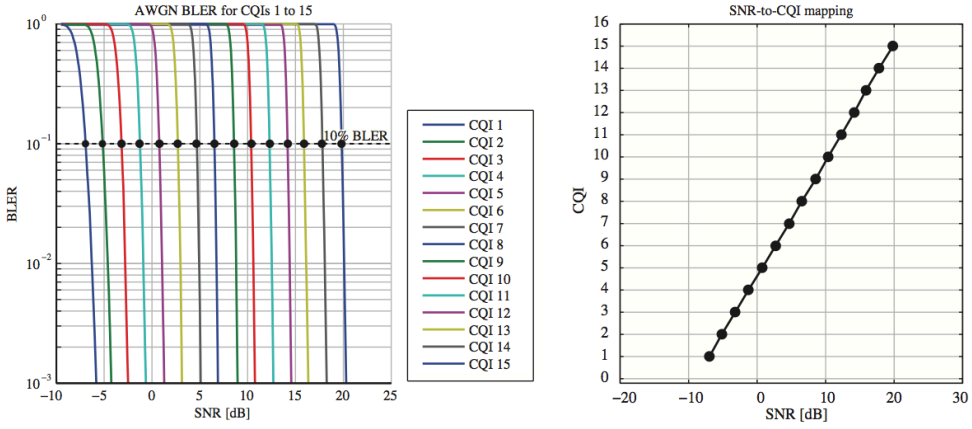

Figure 19 - CQI vs. BLER curves (left) and CQI from the 10% BLER points (right) [18]

5.1.1. Using the simulator

The objetive of this part of the work is to obtain the BLER traces of a specific UE. The configuration parameters are in table 3. The reasons of choosing this parameters is described in sections 6 and 7.

PARAMETER	VALUE
Simulation length	30 s
Network details	- 7 macro cells (trisector each one) with radius equal to

	0.5 km; - number of user in each cell: chosen in the range [5, 30]; - speeds chosen between 5 km/h, 36 km/h and 72 km/h; - mobility model: straigh model, random direction
Physical detail	- Carrier Frequency: 2 GHz; - Bandwidth for the DL: 10 MHz; - Antenna system: MIMO 2x1 with Closed Loop Spatial Multiplexing; - Modulation Scheme: 16-QAM; - Propagation loss model: urban; - eNodeB power transmitted: 40 dBm;
Protocol Overhead	- RTP/UDP/IP with ROHC compression: 3 bytes; - MAC and RLC: 5 bytes; - PDCP: 2 bytes - CRC: 3 bytes - L1/L2: 3 symbols;

Table 3 - Configuration parameters of the System Simulator

The network is represented in figure 20 (corresponded to 30 UEs per eNodeB):

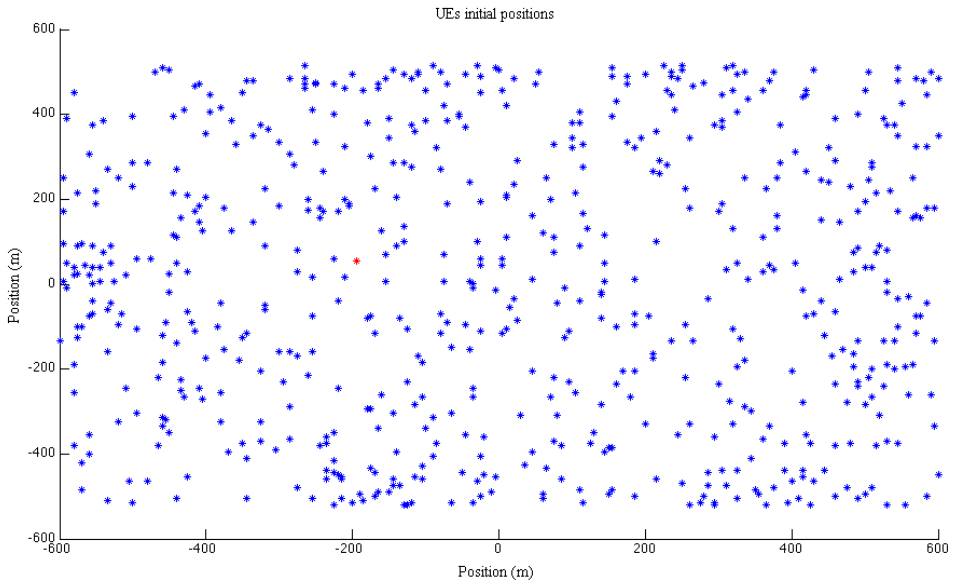

Figure 20 - UEs network configured (30 UEs per eNodeB)

Where the blue points represents the initial position of the UEs at the begin of the simulation. The red point represents the initial position of the studied UE. The positions of the trisector eNodeBs (base stations) are represented in figure 21:

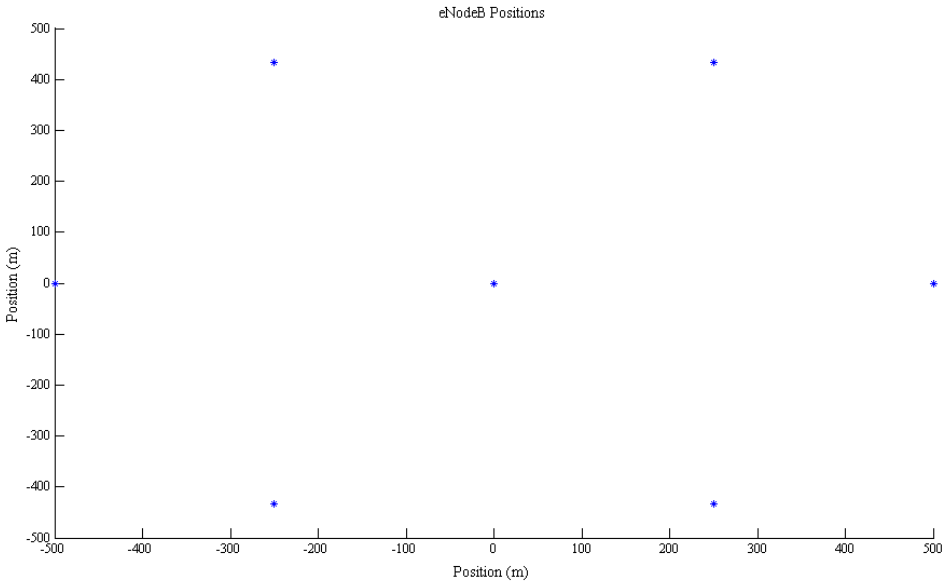

Figure 21 - Base station positions

The positions of the studied UE are represented in the next three figures, one for each speed. The red trace represents the evolution of the studied UE position during the simulation.

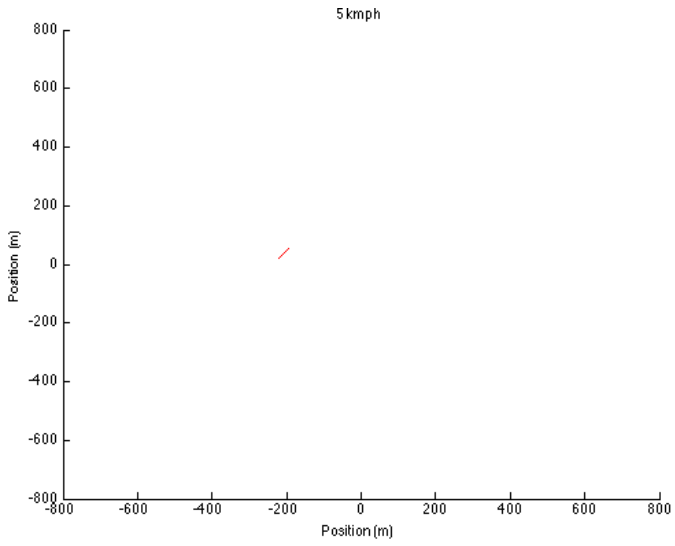

Figure 22 - UE positions for 5km/h

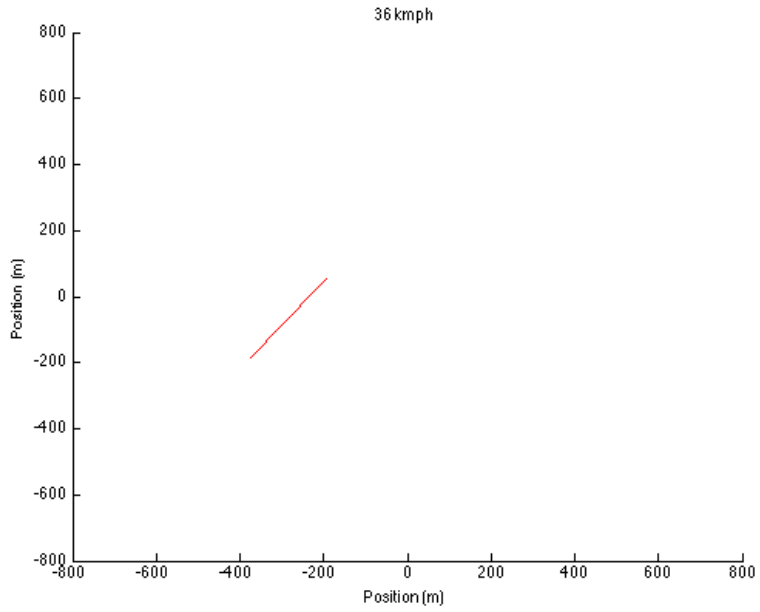

Figure 23 - UE position for 36km/h

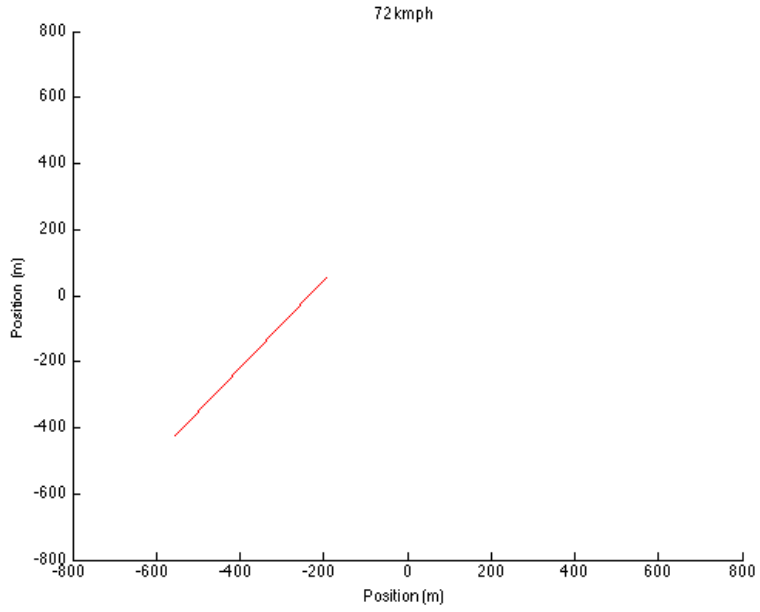

Figure 24 - UE positions for 72km/h

It can be appreciated in the figures that the studied UE direction is 233°.

5.2. Evaluated scenarios

It could be represented a diagram of the evaluated scenario in this work:

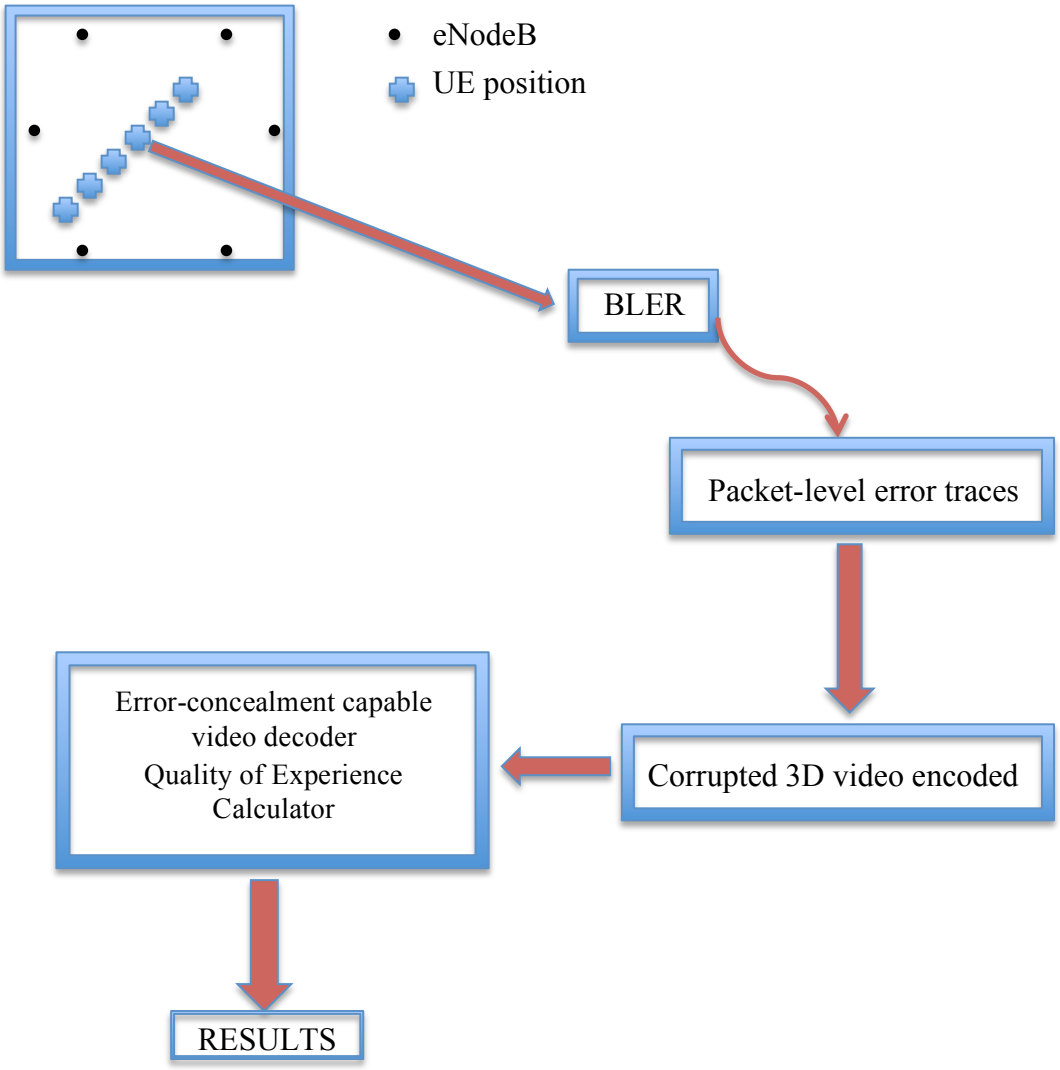

Figure 25 - Diagram of the evaluated scenario

Thus, after obtaining the Block Error Rate for the UE during the simulation, the BLER trace was converted to a packet level error trace (binary error trace). For this purpose, firstly the BLER trace (with its respective block length –in this case, 6-) is converted to a Bernoulli sequence of packet loss events. The next step is, given a file of lengths (in bits) of compressed 3D video file and the Bernoulli sequence mentioned, create a binary sequence of packet level error traces.

The Bernoulli sequence provides a sequence of packet error trace. Thus, given the system-layer transport block sizes (as mentioned, it changes dynamically) and the lengths of the 3D video file packets, it is possible to know the amount of system-layer packets that forming each 3D video file packet. Figure 26 shows an example:

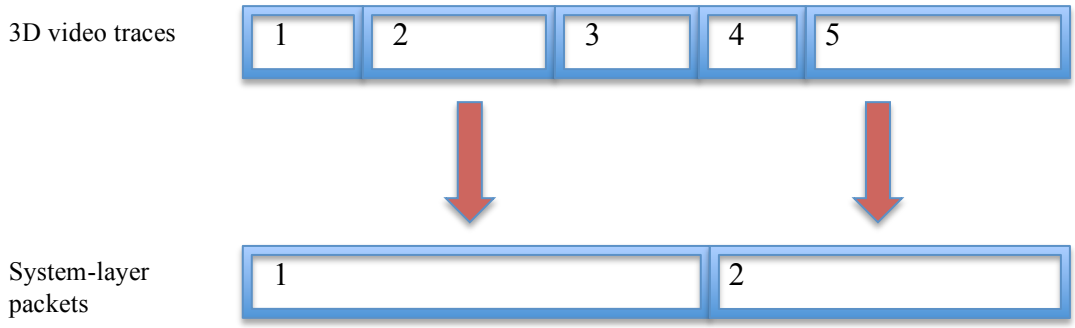

Figure 26 - System-layer packets and 3D video traces

Once obtained this information, based on the Bernoulli sequence, in order to create the packet level error trace the decision was basically establish an error packet if this packet had any loss.

Figure 27 shows the structure of this conversion:

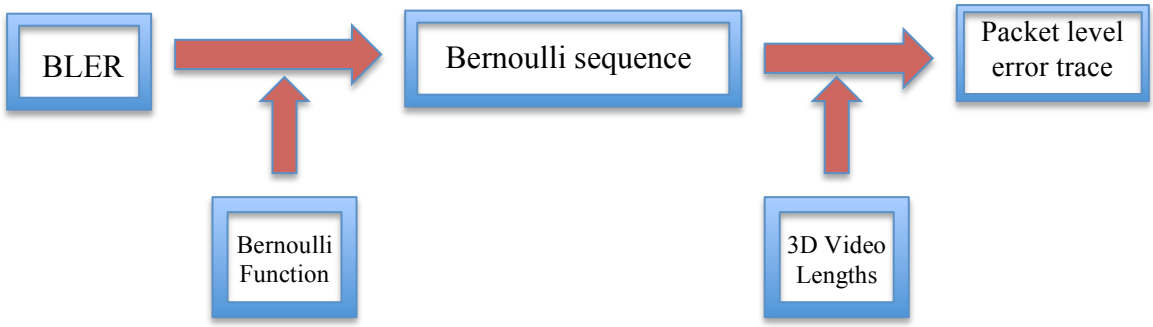

Figure 27 - Block Diagram of the BLER conversion

The corrupted encoded video stream will be decoded using an error-concealment capable video decoder and the decoded/recovered video quality (QoE) will be estimated based on the Structural Similarity Index of the recovered video. This last block is not in the scope of this work; please refer to [11] for further information.

6. Experiments and results

As mentioned before, three different user speeds were simulated: 5 km/h (1.38 m/s), 36 km/h (10 m/s) and 72 km/h (20 m/s). The main purpose of using this values is that 5 km/h is the minimum user speed available in the simulator. The other two values are realistic in an urban environment (e.g. user travelling in a car).

Four different 3D video coded files where corrupted to obtain the results: *kendo*, *balloons*, *lovebird* and *newspaper*. The analysis of this files is out of the scope of this work, in [11] it is highly analyzed. Table 4 shows the encoder setting parameters of the videos used:

3D video (spatial resolution)		**Bitrate (kb/s)**	**Bit budget (%)**	**Average PSNR (dB)**
Balloons (1024x768)	Tex.	1095	84.8 %	41.41
	Dep.	196	15.2 %	39.47
Kendo (1024x768)	Tex.	1173	79.6 %	42.45
	Dep.	300	20.4 %	38.40
Lovebird (1024x768)	Tex.	825	89 %	39.17
	Dep.	102	11 %	42.32
Newspaper (1024x768)	Tex.	935	85.5 %	39.28
	Dep.	150	14.5 %	39.08

Table 4 - Encoder setting parameters of the videos used

Where the *bit budget* column represents the amount of space in the encoded packet occupied by the texture packet or the depth packet, respectively.

In order to understand better the results, first the results of the *intermediate stage* (the simulator output results) will be shown.

6.1. Simulator output results

6.1.1. Balloons

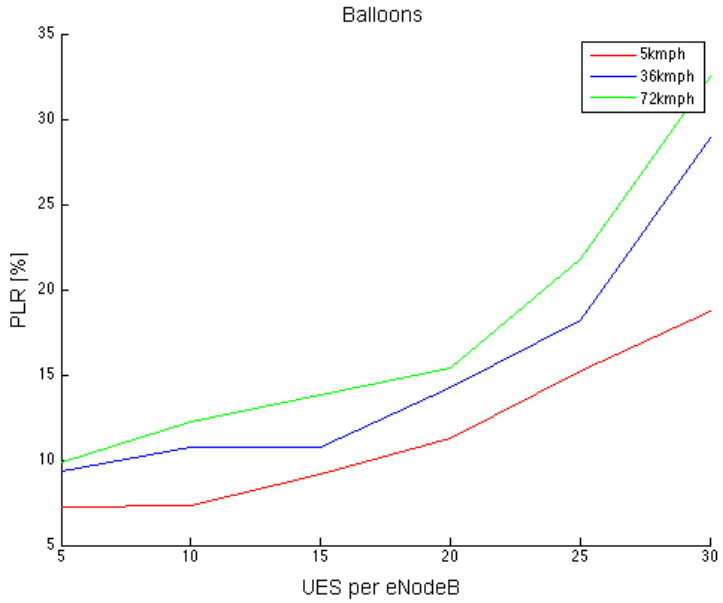

Figure 28 - PLR results for Balloons

6.1.2. Kendo

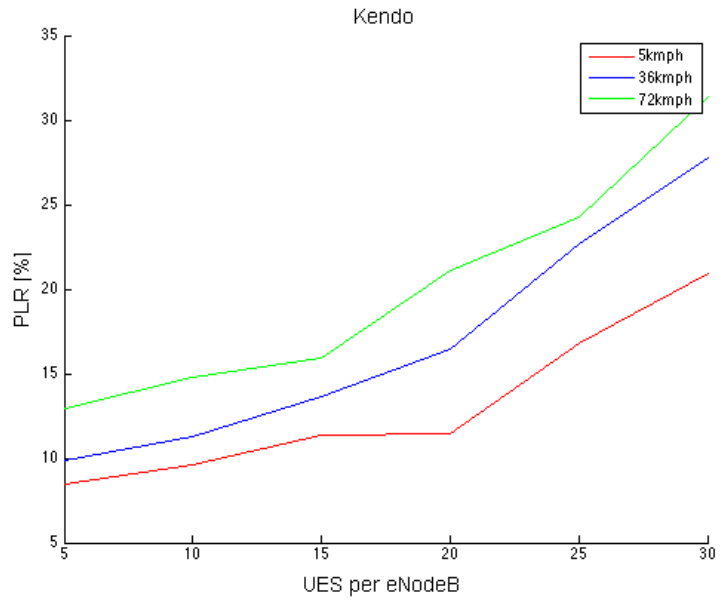

Figure 29 - PLR results for Kendo

6.1.3. Lovebird

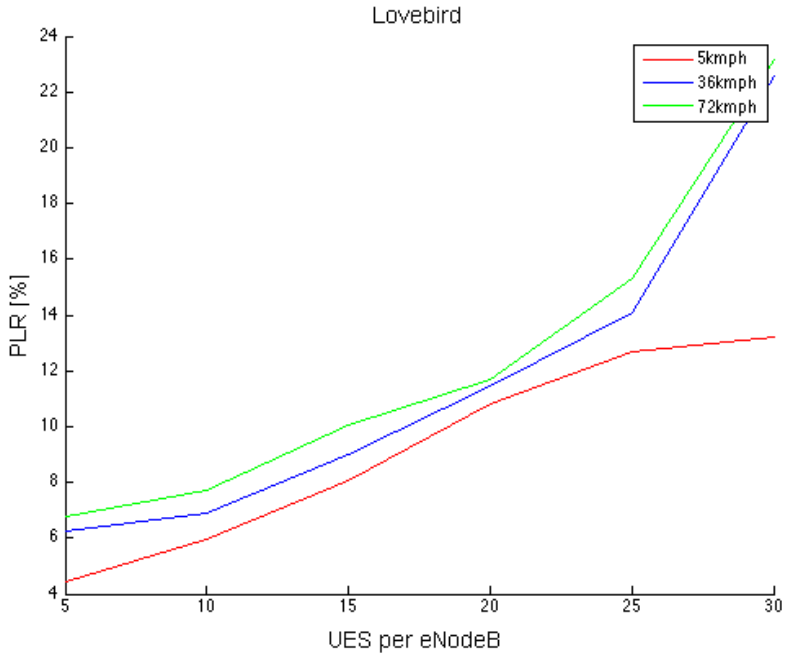

Figure 30 - PLR results for Lovebird

6.1.4. Newspaper

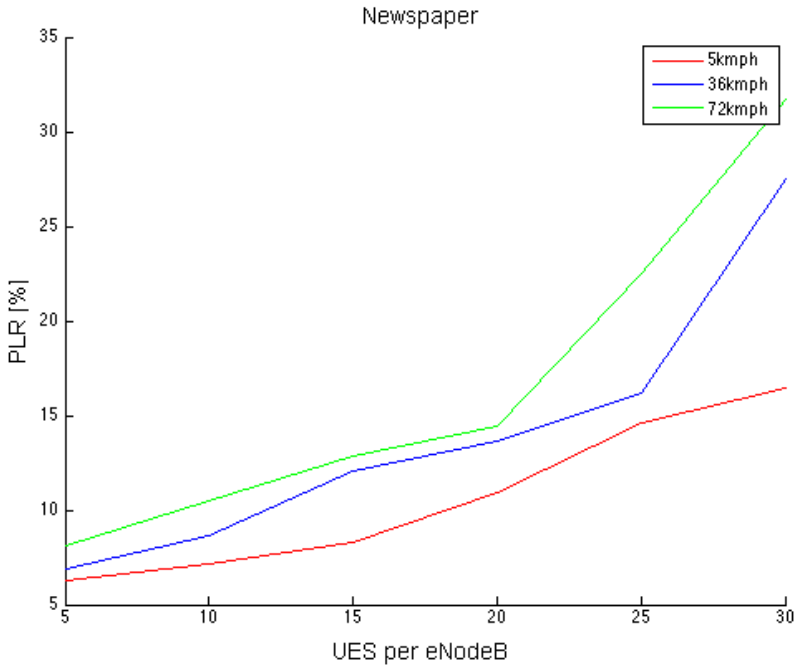

Figure 31 - PLR results for Newspaper

6.1.5. Overview

The next 4 tables show the numeric data of the PLR, one for each video file.

Balloons

UEs per eNodeB / UE speed	5	10	15	20	25	30
5 km/h	7.2291	7.2916	9.2083	11.2916	15.1875	18.6875
36 km/h	9.3541	10.7083	10.7083	14.2708	18.2291	28.8958
72 km/h	9.875	12.2708	13.7916	15.3750	21.7916	32.5208

Table 5 - PLR results from Balloons

Kendo

UEs per eNodeB / UE speed	5	10	15	20	25	30
5 km/h	8.4166	9.6250	11.3968	11.4583	16.7708	20.9166
36 km/h	9.8750	11.2291	13.6458	16.4375	22.6458	27.7708
72 km/h	12.896	14.7916	15.9375	21.1041	24.2708	31.3750

Table 6 - PLR results from Kendo

Lovebird

UEs per eNodeB / UE speed	5	10	15	20	25	30
5 km/h	4.4010	5.9375	8.0468	10.8333	12.6562	13.2292
36 km/h	6.2500	6.8750	9.0104	11.4323	14.1146	22.6458
72 km/h	6.7448	7.7083	10.0264	11.6666	15.3385	23.1250

Table 7 - PLR results from Lovebird

Newspaper

UEs per eNodeB / UE speed	5	10	15	20	25	30
5 km/h	6.2916	7.1666	8.3125	10.8958	14.5833	16.4375
36 km/h	6.8750	8.6259	12.0625	13.6458	16.1666	27.5120
72 km/h	8.0625	10.4792	12.8333	14.4166	22.4791	31.6666

Table 8 - PLR results from Newspaper

After being shown the results of the *intermediate stage*, the output final results will be given in the next subsection, as well as the analysis of them.

6.2. QoE results

After obtaining the PLR results and extract the Block Error Rate, the BLER sequences were converted to packet level error traces and used to corrupt the 3D codec video files.

The QoE results of this files are shown in the next four figures:

6.2.1. Balloons

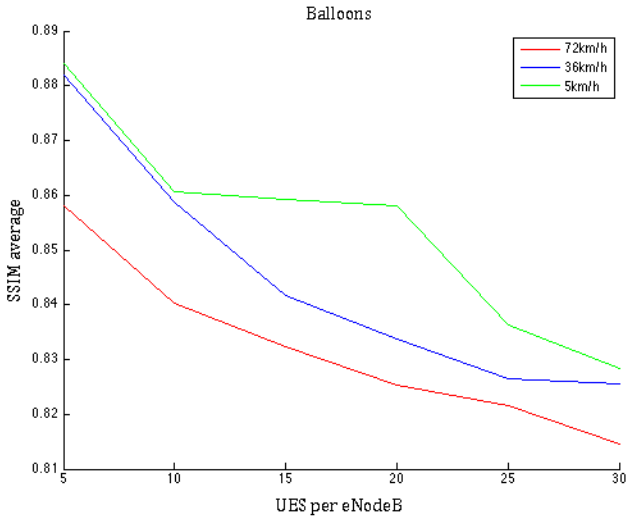

Figure 32 - QoE results for Balloons

6.2.2. Kendo

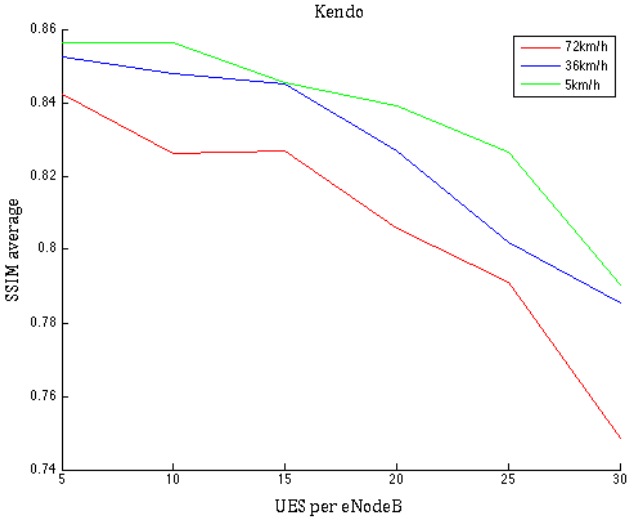

Figure 33 - QoE results for Kendo

6.2.3. Lovebird

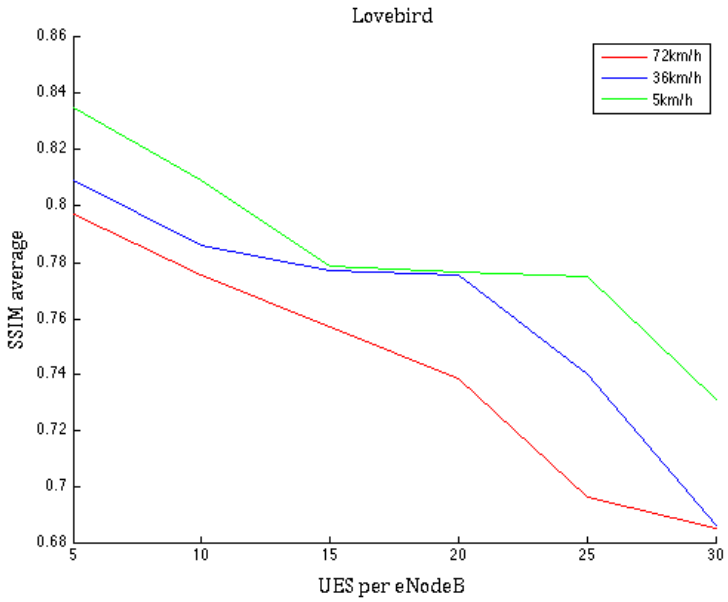

Figure 34 - QoE results for Lovebird

6.2.4. Newspaper

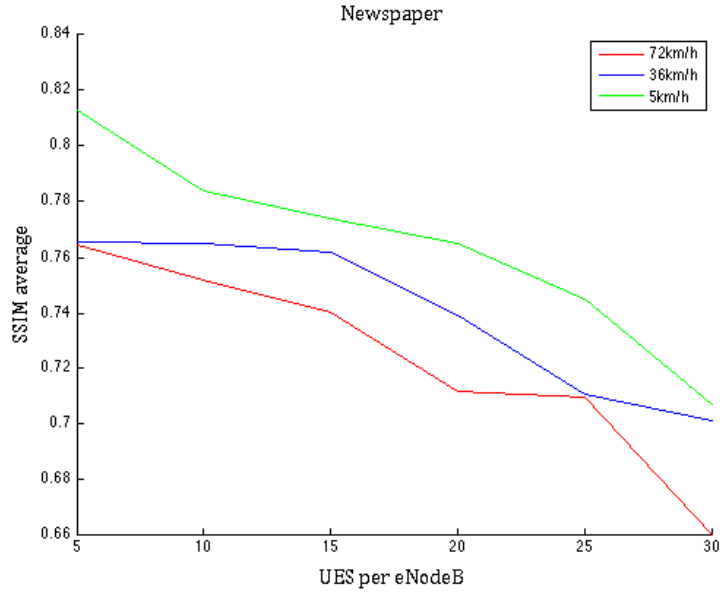

Figure 35 - QoE results for Newspaper

6.2.5. Overview

The next table shows the numeric data of the Structural Similarity Index (SSIM).

Balloons

UEs per eNodeB / UE speed	5	10	15	20	25	30
5 km/h	0,8841	0,8606	0,8593	0,8581	0,8362	0,8284
36 km/h	0,8820	0,8587	0,8417	0,8336	0,8264	0,8256
72 km/h	0,8581	0,8403	0,8322	0,8253	0,8217	0,8146

Table 9 - SSIM results from Balloons

Kendo

UEs per eNodeB / UE speed	5	10	15	20	25	30
5 km/h	0,8563	0,8564	0,8455	0,8391	0,8266	0,7904
36 km/h	0,8525	0,8479	0,8449	0,8269	0,8019	0,7852
72 km/h	0,8424	0,8262	0,8270	0,8059	0,7909	0,7485

Table 10 - SSIM results from Kendo

Lovebird

UEs per eNodeB / UE speed	5	10	15	20	25	30
5 km/h	0,8354	0,8092	0,7785	0,7768	0,7752	0,7313
36 km/h	0,8092	0,78628	0,77705	0,7754	0,7401	0,6868
72 km/h	0,7972	0,7754	0,75707	0,7386	0,6965	0,6855

Table 11 - SSIM results from Lovebird

Newspaper

UEs per eNodeB / UE speed	5	10	15	20	25	30
5 km/h	0,8129	0,7841	0,7738	0,7652	0,7452	0,7070
36 km/h	0,7655	0,7651	0,7616	0,7392	0,7106	0,7013
72 km/h	0,7647	0,7520	0,7403	0,7120	0,7098	0,6605

Table 12 - SSIM results from Newspaper

6.3. Analysis of the results

The simulation results are consistent with expectations. It can be seen that the Packet Loss Ratio (PLR) increases with user speed. As mentioned before in this work, LTE is optimized for low speeds (to about 15 km/h). At higher speeds, due to the multipath propagation, interference and handover delay effects, the communication will suffer losses.

Thus, if the user is walking (around 5 km/h), the LTE transmission shouldn't suffer too many losses (in this case, PLR values are situated between 4% and 12%). On the other hand, if the user speed is incremented, the LTE transmission will start to experience losses in the link, with a PLR ranging between 13% and 32%.

Moreover, relative to network users density, the PLR increases also users density. It is also expected: if there are more active users in the network, the link level error will increase.

In terms of Structural Similarity Index (SSIM), it takes places the opposite of PLR evolution. This is also consistent with expectations: if the user speed increases, the SSIM will be decreased; and if the network user density tends to grow, the SSIM will fall.

7. Conclusion

In this thesis, the main goal was to perform the simulation of losses of compressed 3D video transmitted over an LTE system.

The first step, study the simulator capabilities and evaluate its behavior into our problem, was successfully achieved. Firstly it was tested the Link-Level simulator, but finally it was discarded because it didn't comply with the main purpose. After simulating different scenarios, finally the System-Level was used. It is critical to establish a realistic simulated scenario, so the first issue to overcome was to decide the simulation length, and the transmit mode in LTE. The simulation length, after studying deeply the simulator, was fixed in 30 seconds, and the transmit mode in MIMO 2x1 (mentioned before), because MIMO is the main transmit mode in LTE nowadays.

It's important to take account the limits of the 3D video corrupter, because it can't be able to analyze data frames with bandwidth upper to 1.4 MHz and with modulations higher than 16-QAM. Therefore, these limits were the simulation limits.

Then, the output results of the simulations were studied. Since it was found that the output frames didn't provide the packet level error traces, it was performed a program in order to convert this BLER sequences to packet level error traces (mentioned before in this work).

Finally it was obtained the packet level error traces of a single UE during the simulation, so the main goal of this thesis was successfully achieved.

The best QoE results are those corresponding to the speed of 5 kilometers per hour and 5 users per base station, and the worst ones are those corresponding to the speed of 72 kilometers per hour and 30 users per base station. The network congestion and the user speed cause losses in the LTE transmission, as mentioned before.

The observed results show the dependency of the QoE on the increase of the number of LTE users and user speed. As a final conclusion, it can be argued that the work presented complies with the initial objectives.

It’s difficult to evaluate the QoE of a 3D video in a LTE transmission objectively. Furthermore, the quality references are continuously changing due to the advances of technology. However, these simulations can help to infer the relationship between the system configurations (user densities, user velocities) and the achievable QoE.

As a future work, it could be suggested a study based on the comparison between the encoder setting parameters of the four 3D video coded files and the QoE obtained during the simulation in this dissertation.

The evolution in 3D technologies and the next LTE release will certainly cause an important growth in the use of these technologies in mobile networks. The next step in video technologies is the evolution for 2D video to 3D video, because it increases the user experience.

Therefore, the task of the engineering will be developing the 3D technologies in mobile networks, because the demand is continually growing.

References

[1] E. Dahlman, S. Parkvall, J. Sköld and P. Beming, "3G Evolution: HSPA and LTE for Mobile Broadband", Elsevier, 2007.

[2] E. Dahlman, S. Parkvall and J. Sköld, "4G LTE/LTE-Advanced for Mobile Broadband", Elsevier, 2011.

[3] A. F. Molisch, "Wireless Communications", 2nd Edition, 2011.

[4] Campus Sur de la Universidad Politécnica de Madrid, "Capa Física y Planificación en LTE", in *LTE: Long Term Evolution*, 2013.

[5] J. Zyren, "Overview of the 3GPP Long Term Evolution Physical Layer", Freescale Semiconductor, 2007.

[6] T. Kim, J. Kang, S. Lee and A. C. Bovik, "Multimodal Interactive Continuous Scoring of Subjective 3D Video Quality of Experience", *IEEE Transactions on Multimedia*, vol. 16, no.2, Feb. 2014.

[7] S. Singh, O. Oyman, A. Papathanassiou, D. Chatterjee and J.G. Andrews, "Video capacity and QoE enhancements over LTE", *IEEE International Conference on Communications (ICC)*, Jun. 2012.

[8] J. Gautier, E. Bosc and L. Morin, "Representation and coding of 3D video data", in *Schémas Perceptuels et Codage video 2D et 3D*, Feb. 2011.

[9] L. Rocha and L. Gonçalves, "An Overview of Three-Dimensional Videos: 3D Content Creation, 3D Representation and Visualization", Intech, 2012.

[10] G. Piuro, C. Ceglie, D. Striccoli and P. Camarda, "3D video transmissions over LTE: a performance evaluation", *IEEE EUROCON Conference*, Jul. 2013.

[11] J. R. Simões Soares, "Quality Evaluation of 3D Video Subject to Transmission Channel Impairments", Dissertação de Mestrado, Sept. 2013.

[12] M. Lee, J. Lee and H. Lee, "Perceptual Watermarking for 3D Stereoscopic Video using Depth Information", *2011 Seventh International Conference on Intelligent Information Hiding and Multimedia Signal Processing*, Sept. 2011.

[13] C. T. Hewage and M. G. Martini, "Quality evaluation for real-time 3D video services", *IEEE International Conference on Multimedia and Expo (ICME)*, Jul. 2011.

[14] R. Radhakrishnan and A. Nayak, “Cross layer design for efficient video streaming over LTE using scalable video coding”, *IEEE International Conference on Communications (ICC)*, Jun. 2012.

[15] Daribo, “An interactive depth-based multi-view system for 3DTV”, Keio University, Oct. 2012.

[16] C. Ikuno, M. Wrulich and M. Rupp, “System Level Simulation of LTE networks”, *IEEE 71st Vehicular Technology Conference*, May. 2010.

[17] C. Mehlführer, J. C. Ikuno, M. Simko, S. Schwarz, M. Wrulich and M. Rupp, “The Vienna LTE Simulators – Enabling Reproducibility in Wireless Communications Research”, *EURASIP Journal on Advances in Signal Processing*, 2011.

[18] C. Ikuno, “Vienna LTE Simulators: System Level Simulator Documentation, v1.7r1119”, Institute of Telecommunications of Vienna University of Technology, March 2013.

[19] Zeng and Z. Wang, “3D-SSIM for Video Quality Assessment”, *IEEE International Conference on Image Processing (ICIP12)*, Sept. 2012.

[20] Z. Wang, A. C. Bovik, H. R. Sheikh, and E. P. Simoncelli, “Image quality assessment: From error visibility to structural similarity,” IEEE Trans. Image Processing, vol. 13, no. 4, pp. 600–612, April 2004.

[21] H. Pinson and S. Wolf, “A new standardized method for objectively measuring video quality,” *IEEE Trans. Broadcasting*, vol. 50, no. 3, pp. 312–322, September 2004.

[22] K. Seshadrinathan and A.C. Bovik, “Motion tuned spatiotemporal quality assessment of natural videos,” *IEEE Trans. Image Processing*, vol. 19, no. 2, pp. 335–350, Feb. 2010.

[23] J. You, J. Korhonen, A. Perkis, and T. Ebrahimi, “Balancing attended and global stimuli in perceived video quality assessment,” *IEEE Trans. Multimedia*, vol. 13, no. 6, pp. 1269–1285, Dec. 2011.

[24] M. Nasralla, O.Ogneoski and M.G. Martini, “Bandwidth Scalability and Efficient 2D and 3D Video Transmission over LTE Networks”, *IEEE International Conference of Communications”*, 2013.

[25] M. Sauter, “From GSM to LTE: an introduction to mobile networks and mobile broadband”, *WirelessMoves*, Wiley Ed., 2011.

[26] P. Rysavy, “Transition to 4G: 3GPP Broadband Evolution to IMT-Advanced (4G)”, Rysavy Research, 2010.

[27] D. Flore, “LTE RAN Architecture Aspects”, Qualcomm Inc, 2010.

[28] S. Geirhofer, A. Farajidana and T. Ji, “DL MU-MIMO operation in LTE-A”, Qualcomm Incorporated, 2011.

[29] A. Narula, M. Trott and G. Wornell, “Performance Limits of Coded Diversity Methods for Transmitter Antenna Arrays”, *IEEE Transactions on Information Theory*, vol. 45, no. 7, Nov. 1999.